"Compartment specific mitochondrial dysfunction in Drosophila knock-in model of ALS reversed by altered gene expression of OXPHOS subunits and pro-fission factor Drp1"

Y Nemtsova[1], BL Steinert[1,*], KA Wharton[1,2]

[1]Molecular Biology, Cell Biology, and Biochemistry Department, Brown University, Providence, Rhode Island 02912, United States.

[2]Robert J. and Nancy D. Carney Institute for Brain Science, Brown University, Providence, Rhode Island 02912, United States.

Abstract

Amyotrophic Lateral Sclerosis (ALS) is a fatal multisystem neurodegenerative disease, characterized by a loss in motor function. ALS is genetically diverse, with mutations in genes ranging from those regulating RNA metabolism, like *TAR DNA-binding protein (TDP-43)* and *Fused in sarcoma (FUS),* to those that act to maintain the redox homeostasis of the cell, like *superoxide dismutase 1 (SOD1).* Although varied in genetic origin and in specific cellular defects, there are pathogenic and clinical commonalities between cases of ALS. Defects in mitochondria is one such common pathology, which is thought to occur prior to, rather than as a consequence of symptom onset, making these organelles a promising therapeutic target for multiple neurodegenerative diseases, including ALS. Depending on the homeostatic needs of neurons throughout life, mitochondria are normally shuttled to different subcellular compartments regulating metabolite and energy production, lipid metabolism, and buffering calcium, as well as influencing other essential cellular processes. While initially considered a motor-neuron disease based on the dramatic loss in motor function and motor neuron cell death, studies of ALS have shown molecular and cellular defects in non-motor neurons and glial cells alike, often preceding motor neuron death, suggesting that a disruption in these cell types could initiate and/or facilitate a decline in motor neuron function. Here, we investigate mitochondria in a *Drosophila Sod1* knock-in model of ALS. In depth, *in vivo*, examination reveals innate mitochondrial dysfunction evident prior to motor-symptom onset, with abnormal subcellular distributions of mitochondria in diseased sensory neurons with no apparent defects in the axonal transport machinery. Using genetically expressed biosensors in the context of the intact motor circuit, changes in mitochondrial morphology, oxidative phosphorylation, and mitophagy in sensory neurons are correlated with a reduction in locomotion. We demonstrate that targeted expression of specific electron transport

To whom correspondence should be addressed: Tel +1 4018631951, Fax +1 4018632421, 185 Meeting St, Box G-L, Providence, RI, 02912, Kristi_Wharton@brown.edu.
*Current address: Department of Organismic and Evolutionary Biology, Harvard University, 1 Oxford St #371, Cambridge, MA 02138, United States. bsteinert@g.harvard.edu

chain (ETC) subunits can alleviate ALS-associated defects in mitochondrial morphology and function.

Keywords

neurodegeneration; ALS; mitochondrial dysfunction; sensory neurons; Drosophila

Introduction

Amyotrophic Lateral Sclerosis (ALS) is a debilitating neurodegenerative disease, which currently has no cure. The disease is fatal, with death occurring on average three years post diagnosis, and affecting 3-5 of 100,000 individuals worldwide (Brown, 2017). The specifics of symptom onset varies but typically, focal muscle weakness and wasting is seen in arms, hands, legs, and feet, and gradually spreads throughout the body. About 25-30% of patients present with bulbar onset, with a degeneration of muscles responsible for chewing, swallowing, speech, and jaw movement (Gale Encyclopedia of Medicine, 2008). Cognitive decline is evident in ALS patients, with frontotemporal dysfunction as the leading cause (Phukan et al., 2007). Although motor neurons are profoundly affected especially in the end stages of ALS, defects in skeletal muscle, cortical neurons, glia, and sensory neurons have all been well documented (Cassina et al., 2021; Held et al., 2019; Taylor et al., 2016; Pugdahl et al. 2006; Zanette et al., 2002). Thus, ALS is no longer considered an exclusively motor neuron disease, but manifests itself as a multisystem neurodegenerative disorder, with clinical, cellular, and genetic diversity (Masrori and Damme, 2020; Brown, 2017; Hardiman et al., 2017).

There are many genes associated with ALS, the most common of which include *TAR DNA-binding protein (TDP-43), Fused in sarcoma (FUS)*, chromosome 9 open reading frame 72 (*C9orf72*), and *superoxide dismutase 1 (SOD1)* (Sultan et al., 2016). *SOD1 [Cu-Zn]* was the first of these genes to be associated with ALS and has 208 known mutations linked to ALS pathology (ALSoD, accessed January 2023). *SOD1* encodes an enzyme comprised of 154 amino acids (Sayers et al., 2022) that breaks down reactive oxygen species (ROS), a normal byproduct of cellular metabolism (Chen et al., 2013; Valentine at al., 2005). When left unregulated, ROS reacts with nucleic acids, lipids, metabolites, and proteins compromising their activity (Cooke et al., 2003). Aside from its antioxidant function, SOD1 has also been shown to regulate gene transcription (Chi Kwan et al., 2014), possess anti-apoptotic properties (Valentine et al., 2005), and exhibit peroxidase activity with H_2O_2 as a substrate (Hink et al., 2002). Point mutations in *SOD1* have been shown to cause loss of protein activity, as well as gain of a toxic function that may reflect defects in protein folding, localization, and/or aggregation, in the cytoplasm, and in organelles, such as in mitochondria (Sultan et al., 2016, Tafuri et al., 2015). While some mutations result in a higher propensity for the SOD1 protein to aggregate (Sheng et al., 2012, Valentine et al., 2005), it is clear that ALS pathophysiology displayed by patients, as well as that seen in animal models, is not solely caused by SOD1 aggregation, or necessarily correlated with their presence (Brotherton, Li, and Glass, 2013, Saccon et a., 2013, Prudencio et al., 2009). In fact, more recent studies have concluded that the formation of SOD1 aggregates may be a protective

mechanism against neurotoxic forms, and that there is an inverse correlation between the presence of SOD1 aggregates in tissues most affected by disease (Zhu et al 2018; Gill et al., 2019). A number of SOD1-ALS models demonstrate that affected animals exhibit clear motor dysfunction and cellular defects analogous to those observed in ALS patients (Sahin et al., 2017, Muller at al., 2006). Given the proclivity of nearly any residue of SOD1 to be mutated in ALS, aligned with the variability with which each mutated SOD1 protein aggregates in vivo and/or alters dismutase function, efforts to elucidate the impact of SOD1-based models that exhibit clear neurodegenerative phenotypes will contribute to uncovering mechanisms governing ALS progression.

The connection between mutant SOD1, a cytosolically located protein, and the presence of defective mitochondria is well-recognized in ALS, but the mechanisms underlying their contribution to pathogenesis is poorly understood. To maintain neuronal homeostasis, mitochondria are trafficked along axonal microtubules to areas of the neuron where they are necessary to uphold cellular function, such as in cell bodies during organelle biogenesis when energy demand is high, and to synapses when high calcium buffering is required for axonal restoration following wounding. Mitochondria are localized to specific subcellular compartments when metabolite-, fatty acid-, or cholesterol-biosynthesis are needed (Glancy et al., 2020). Mitochondrial dysfunction has been reported in virtually all neurodegenerative diseases (NDs) and mutations in *SOD1-ALS* have been shown to both directly and indirectly lead to changes in mitochondrial morphology, ultrastructure, fission and fusion dynamics, quality control, metabolic activity, and axonal transport (Velde et al., 2011; De Vos et al., 2007; Magrane et al., 2012; Smith et al., 2017; Palomo and Manfredi, 2014). Mitochondrial defects typically precede disease phenotypes (Baldwin et al., 2016), an observation that makes identifying changes in morphology and function a promising criterion for early detection of ALS, with mitochondria themselves as a target for therapeutic development. The recently approved AMX0035 compound leveraged its effects on mitochondrial and endoplasmic reticulum dysfunction and cell death pathways to reduce loss of neurons (Amylyx Pharmaceuticals Inc., 2021, Clinical trial NCT03127514). Other therapeutic agents that target mitochondria in animal models of ALS, include P110, an inhibitor of DRP1/Fis1 proteins regulating mitochondrial structure; olesoxime, an inhibitor of mitochondrial turnover; and resveratrol, an activator of mitochondrial turnover (Joshi et al., 2018; Martin, 2010; Laudati et al., 2019). In all cases, these agents slow disease progression, albeit mildly. The ability to target mitochondria is promising and with a more complete understanding of the role of mitochondrial pathogenesis in ALS, more effective or of new types of interventions will be possible.

We employed live time-lapse microscopy and immunocytochemistry to assess and quantify mitochondrial dysfunction in a knock-in SOD1 model of ALS in *Drosophila*, and show that this dysfunction can be rescued. We made use of two different *dSod1* knock-in models that contain the glycine 85 to an arginine (G85R) mutation in the highly conserved *Sod1* gene (Sahin et al., 2017; Russo et al, 2023). *dSod1*^{G85R} homozygote animals recapitulate ALS-like phenotypes, such as neurodegeneration and defects in motor function (Sahin et al., 2017; Held et al., 2019), comparable to that observed in ALS patients. These studies revealed abnormalities in the motor circuit of *dSod1*^{G85R} knock-in animals that disrupts the

integrated communication between muscles, motor neurons, and sensory neurons, known to underlie locomotor defects in ALS.

Drosophila melanogaster has proven to be an invaluable tool for modeling a range of NDs (Anoar et al., 2021; Chai and Pennetta, 2015) given the neuronal and genetic conservation across species (Pandey and Charles, 2011). Perhaps most importantly, *Drosophila* models have allowed us to study whole neural circuits and to probe a single neuronal cell type in the context of the intact motor circuit. Our previous electrophysiological analysis of the motor circuit revealed a profound disruption in sensory neuron feedback in $dSod1^{G85R}$-ALS animals and demonstrated that this defect precedes abnormalities at the neuromuscular junction (NMJ) and motor neuron dysfunction that is evident with progressive loss of motor function (Held et al, 2019). Notably, in mammalian systems, ALS-linked disruptions in sensory feedback have been shown to accelerate disease onset, with sensory neurodegeneration evident in ALS patients, as well as in an array of ALS models (Pugdahl et al., 2006; Vaughan et al., 2015; Ilieva et al., 2008). The involvement of non-motor neurons in ALS, especially at early stages, with its apparent contribution to accelerated progression, highlight the multi-cellular systemic degenerative properties of ALS and the need to understand the extent of sensory neuron involvement.

Drosophila sensory neurons are integral to the motor circuit and, as such, are necessary for generating larval peristaltic locomotion, crawling, eclosion, as well as other essential physiological motor behaviors (Kohsaka et al., 2012, Song et al., 2007; Zdarek and Friedman, 1986). Consistent with the importance of sensory neurons in locomotion, coupled with our electrophysiological data indicating defects sensory neuron function in $dSod1^{G85R}$ ALS animals, our results reveal that mitochondria in multidendritic (MD) neurons, a well-characterized subset of sensory neurons, exhibit severe morphological abnormalities. Live time-lapse imaging detected fewer mobile mitochondria in MD axons. Furthermore, we found that distinct subcellular compartments of MD neurons in $dSod1^{G85R}$ animals showed differences in the abundance, function, and turnover of mitochondria, based on *in vivo* analyses using genetic biosensors. Interestingly, we found that the reduced number of mobile mitochondria in axons of $dSod1^{G85R}$ animals must not result from defects in the axonal transport machinery, but most likely from an innate defect in the organelle itself. Consistent with this conclusion, we showed that the targeted expression of specific electron transport chain (ETC) subunits can restore organelle and neuronal function. Together, we reveal the molecular underpinnings of sensory neuron mitochondrial dysfunction, a novel avenue for studying ALS pathogenesis and provide new targets for specific therapeutic discovery.

Materials and Methods

Drosophila strains, staging, and dissections

All flies were raised at 25°C on standard food containing cornmeal, agar, sugar, inactive yeast and 0.32% Tegosept. For all experiments, 3 virgin female flies were crossed to 2 male flies in glass vials and brooded daily. $dSod1^{WT-loxp}$ and $dSod1^{G85R-hr}$ were generated by homologous recombination (Sahin et al., 2017) and $dSod1^{WT-cr}$ and $dSod1^{G85R-cr}$ were generated by CRISPR-Cas9 editing (Russo et. al., 2023), allowing us to test and

compare two independently generated $dSod1^{G85R}$ models. It is important to note that the $dSod1^{G85R-hr}$ locus contains an additional missense mutation at nucleotide position 1013 with an A to C substitution that appears to be a natural polymorphism present in $dSod1^{WT-loxp}$ that alone does not appear to alter $dSod1$ function or elicit a phenotype (Sahin et al., 2017; Phillips et al., 1995). $dSod1^{WT-cr}$ shares an identical genetic background with $dSod1^{G85R-cr}$. The majority of homozygous $dSod1^{G85R}$ adults (pharates) fail to emerge from their pupal case in a process known as eclosion. Any $dSod1^{G85R}$ adults that eclose (<2%), exhibit severe locomotor deficits and die within a few hours (Sahin et al., 2017; Held et al., 2019; Russo et al., 2023). Third instar $dSod1^{G85R}$ larvae exhibit locomotor defects associated with reduced peristaltic muscle contractions (Held et al., 2019). MD-Gal4 (P{GawB}109(2)80) drives expression in the multidendritic neurons of the PNS (Hughes and Thomas 2007), OK6-Gal4 drives expression in motor neurons (Sanyal, 2009). The mitochondria-specific redox-sensitive GFPs, $mito$-$roGFP$-$Grx1$ and $mito$-$roGFP$-$Orp1$ biosensors are described in Albrecht et al., 2011. Further, UAS-$mito$-QC is a pH-sensitive fluorescent biosensor is used to analyze mitophagy (Lee et al., 2018; Garriga et al., 2020). Any other strains obtained from Bloomington Drosophila Stock Center are listed in Table 1 with identifying BDSC #.

For dissections, early third instar larvae, picked out of the food >72hours AEL (after egg lay), were identified by size and by the presence of un-everted anterior spiracles. Wandering third instar larvae were picked from the side of the vial >96hours AEL, identified by size and un-everted anterior spiracles. Unless stated otherwise, all dissections were performed on wandering 3rd instar larvae in at least triplicate/experiment. Larvae were first washed with 1X phosphate buffered saline (PBS) containing 137mM NaCl, 2.7mM KCl, 10mM Na_2HPO_4, and 1.8mM KH_2PO_4. The wash was performed to remove excess food and larvae were fileted to expose and leave intact, the brain, ventral nerve cord (VNC), axons, and body wall muscles, while removing all other internal organs and the anterior- (head skeleton, mouth parts) and posterior- (posterior spiracles, anal pads) most structures.

Immunohistochemistry:

Dissected larvae were fixed with 4% paraformaldehyde (PFA) and 0.3% PBT (1X PBS and 0.3% Triton) for 15min. The samples were washed 3X with 0.3% PBT and then blocked in NGS for 2hours at RT or overnight at 4C. Filets were incubated with 500mL primary antibodies overnight at 4C on a shaker, washed 3X, and incubated with secondary antibodies for 2hours at RT on a shaker, and finally stained with 1ug/mL Hoechst 33342 (Molecular Probes) for 10min at RT. Following immunohistochemistry, samples were mounted in 80% glycerol 0.5% N-propylgalate mounting media. Antibody dilutions: anti-GFP (chicken, Invitrogen cat# A10263) 1:500, anti-HRP-647 (goat, Jackson labs cat# 123-605-021) 1:500, anti-RFP (rabbit, Rockland cat# 600-401-379) 1:500, goat-anti-chicken 488 (Invitrogen cat# A11039) 1:200, goat-anti-rabbit 594 (Molecular Probes cat# A11012) 1:200. For roGFP2 experiments, dissected samples were incubated for 10minutes in 20mM NEM, and then fixed in PFA (Albrecht et al., 2011). 10mM DTT incubations are done for 2 minutes when necessary.

All fluorescent imaging was performed using a Zeiss LSM 800 confocal microscope. Images to assess mitochondrial morphology were captured under 63Xoil with 0.22um slices, and processed according to the Fiji plugin, Mitochondrial Analyzer (Chaudhry et al., 2020). Presets for 3D thresholding were done using a 0.22 rolling (microns), 1.75 block size, and a C-Value of 5. All measurements normalized to either synaptic ROI, with synaptic regions A3-A6 from both hemisegment of the VNC, or cell body ROI, measurements are for GFP-positive puncta (particles); data shown as percent of control. Images of synaptic regions and cell bodies shown in the figures are 3D reconstructions of thresholded images via the 3D volume plugin in Fiji and are provided for qualitative assessment only. For the *mito-ro-GFP2* experiments, the intensity of 405nm and 488nm fluorescence was measured within an ROI, a ratio of 405nm to 488nm was calculated, and normalized to the ROI; data plotted as a percent of experimental 405/488 ratio to control ratio.

Live imaging:

Dissections were performed on live larvae in Schneider's Drosophila Medium and imaged with an Olympus FV1000 MPE Multiphoton. Videos of transport in the prominent A6-axon at 0.84 seconds/frame, 400 frames, were processed into kymographs through Fiji. The following steps were taken in Fiji for kymograph generation: plugins > registration > correct 3D drift; crop 450 x 35px; image > stacks > reslice > 1.52 output spacing; image > stacks > Z-project > Max intensity. Kymographs are generated from blinded video datasets and scored for stationary, retrograde, and anterograde movement. Velocities were quantified from the slope of retrograde and anterograde mitochondrial movement in kymographs.

Statistical analyses

Statistical analyses on more than two genotypes are conducted in GraphPad Prism by use of ANOVA with Tukey's multiple corrections for normally distributed data and a Kruskal-Wallis test with Dunn's correction for nonparametric data. Statistical analyses on only two genotypes are performed with an unpaired Students t-test for normally distributed data, and a Mann-Whitney test for nonparametric data.

Results

Number of mobile mitochondria reduced in axons of *dSod1*^{G85R} ALS model

Disruptions in mitochondrial trafficking and innate mitochondrial function are commonly reported in neurodegenerative diseases (NDs) like ALS (Obrador et al., 2020; Mishra and Chan, 2014; Schapira and Cooper, 1992). The knock-in *dSod1*^{G85R} ALS model exhibits a progressive loss in motor function, degeneration of motor neurons and the neuromuscular junction (NMJ), coupled with a disruption in electrophysiological properties of both motor and sensory neurons (Sahin et al., 2017; Held et al., 2019; Russo, et al., 2023). Our previous studies have shown that the earliest motor defect correlates with a disruption in neurotransmission within the motor circuit that represents sensory neuron feedback. This disruption in the sensory neuron precedes abnormal electrophysiological properties which ultimately appear and correlate with motor neuron degeneration, NMJ fragmentation, and death (Held et al., 2019). We sought to better understand the cellular basis of the early sensory neuron defect and made use of mito-GFP, a GFP localized to the

mitochondria via a mitochondrial import signal (Pilling & Saxton 2004, RRID:BDSC8443), to visualize neuron-specific mitochondria *in vivo* by live imaging in the $dSod1^{G85R}$ ALS model. Mitochondria were visualized in multidendritic (MD) neurons, a group of well characterized sensory neurons, using the Gal4-UAS system to drive expression of mito-GFP (*MD-Gal4, UAS-mito-GFP*; Duffy 2002). MD-specific mitochondria were visualized in live preparations (larval filets) of the intact larval motor circuit. We used time-lapse microscopy to quantify the number of mitochondria in the segmental nerve that innervates muscles in abdominal segment A6 (Fig 1A, A'). Quantifications showed that the total number of mobile mitochondria in MD axons is reduced in $dSod1^{G85R}$, with no change in the total number of stationary mitochondria compared to controls (Fig 1B-C, Supp Videos WT_1.0, WT_2.0, G85R_1.0, G85R_2.0). The number of mobile mitochondria in $dSod1^{G85R}$ MD axons is lower in both the retrograde and anterograde direction (Fig 1C).

Compartment specific change in mitochondria $dSod1^{G85R}$ neurons

We next quantified mitochondrial content in different subcellular compartments of MD neurons, at synaptic termini and in MD cell bodies by measuring mito-GFP-positive particles (Fig 1D,E, Supp Video SynapticMitochondria_1.0). A cluster of MD sensory neuron cell bodies ddaF, ddaE, ddaD, ddaC, ddaB, and ddaA, the class IV dendritic arborization (da) neurons (Hughes and Thomas, 2007), reside in the periphery within the segmented body wall musculature (Fig 1E) and make synaptic connections with motor and interneurons within the neuropil of the ventral nerve cord (VNC), lateral to the dorsal midline (Hughes and Thomas, 2007). $dSod1^{G85R}$ mutants showed a reduction in mitochondrial content in this synaptic region when compared to $dSod1^{WT}$ animals (Fig 1D). In contrast, mitochondrial content is elevated at the motor neuron synapse, the neuromuscular junctions (NMJ), in $dSod1^{G85R}$, as evidenced by the elevation of mito-GFP-positive particles in NMJ 6/7 in abdominal segment A2 (Fig 1F,F'). No change in mitochondrial content was detected within the cluster of MD da neuron cell bodies (Fig E,E') or the motor neuron cell bodies between $dSod1^{G85R}$ and $dSod1^{WT}$ (Fig 1G,G'). The high number of mito-GFP particles in the motor axons did not allow sufficient resolution to quantify mobile vs stationary mitochondria in motor neurons.

While mitochondrial content in the da cluster of MD neurons was unchanged in $dSod1^{G85R}$ (Fig 1E'), the dendritic tree of the ddaE MD neuron was found to cover a larger area than seen in wild type, as evidenced by an increase in branch lengths, even though the total area of the MD cell bodies themselves was not different between $dSod1^{WT}$ and $dSod1^{G85R}$. The density of mitochondria in ddaE dendrites was unchanged, but an overall increase in the number of mitochondria in the dendritic tree of $dSod1^{G85R}$ is seen given the overall larger dendritic area (Supp 1).

Our previous findings that show sensory neuron function is compromised prior to the degeneration of motor neurons (Held et al., 2019), coupled with the reduced number and altered subcellular distribution of mitochondria in $dSod1^{G85R}$ MD neurons, led us to focus our investigations on MD sensory to elucidate the nature of mitochondrial defects in ALS-induced neurodegeneration.

Transport of non-mitochondrial cargo unaffected in *dSod1^{G85R}* MD neurons

We considered the possibility that the reduced number of mobile mitochondria in the *dSod1^{G85R}* ALS model may reflect a disruption in the axonal transport machinery, critical for moving healthy mitochondria between the cell body and discrete subcellular compartments in order to provide energy, metabolites, lipid synthesis, and calcium buffering (Mandal and Drerup 2019; Vos, 2010; Verstreken et al., 2005). To determine if general transport was defective, we assayed the transport of two other types of cargo in *dSod1^{G85R}*. Lysosomes were marked by a fusion of lysosomal associated membrane protein 1 to GFP (*LAMP1-GFP*), and vesicles carrying the ANF (atrial natriuretic factor) neuropeptide were marked by *preproANF*-Emerald, with each being expressed and visualized in MD neurons under the control of MD-Gal4. Live-imaging of *LAMP1-GFP* or *preproANF*-Emerald puncta showed no significant differences in the number of retrograde, anterograde, or total mobile puncta in *dSod1^{G85R}* MD axons compared to wildtype (Fig 2A,B). To ensure that our live imaging assay system was sensitive enough to detect transport defects with these specific cargos, we measured retrograde movement of each cargo in a dynein knock down (*Dhc64c-RNAi*). As predicted, the positive control showed retrograde transport was significantly reduced for both LAMP1-GFP and preproANF particles in *MD>Dhc64c-RNAi* MD axons (Fig 2A,B). The number of LAMP1 or preproANF-labelled organelles in specific subcellular compartments were quantified, but no differences were evident in the distribution of total GFP-positive or Emerald-positive puncta in synapses or cell bodies of *dSod1^{G85R}* and *dSod1^{WT}* (Supp 2). Thus, while the number of mobile mitochondria is lower in *dSod1^{G85R}* MD axons, all cargos are not affected.

Active transport of mitochondria is not defective in *dSod1^{G85R}* MD neurons

It is possible that the disruption of mitochondrial transport in *dSod1^{G85R}* MD axons reflects a specific defect in the functional output of microtubule motor proteins, i.e., dynein heavy chain (DHC), and kinesin-1 heavy chain (KHC) (Baldwin et al., 2016; Gepner 1996). To test this possibility, we took advantage of known mutations in *Dhc* and *Khc* and tested whether these alleles and *dSod1^{G85R}* exhibit a genetic interaction, an indication that *Dhc* and/or *Khc* function is compromised in the ALS model. In each case, we tested for a genetic interaction by asking if mutant phenotypes associated with *Dhc* or *Khc* were modified by one or two copies of the *dSod1^{G85R}* mutation. *dSod1^{G85R}*/+ heterozygotes alone do not exhibit mitochondrial defects. Mutations in *Dhc64C* are known to decrease dynein ATPase activity (Martin et al., 1999). Live imaging of mito-GFP in MD axons of *Dhc64C^{4-19}*/+ animals showed fewer mobile mitochondria in both retrograde and anterograde directions, a defect not previously reported (Fig 2C, Supp 3). This axonal transport defect observed in *Dhc64C^{4-19}*/+ appears to reflect a dose-sensitive response, since a more significant decrease in mobile mitochondria is evident when silencing DHC activity with *UAS-Dhc64C-RNAi*, akin to reports for *Dhc64C* homozygotes (Reis et al., 2012) (Fig 2C). Given this dose-dependent effect, we tested if the *Dhc64C^{4-19}*/+ phenotype was modified in a *Dhc64C^{4-19} +/+ dSod1^{G85R}* transheterozygous animal. A more severe phenotype would indicate that dynein function is partially compromised in *dSod1^{G85R}* and only revealed in the presence of a dose of the *Dhc64C^{4-19}* mutation. We found no change in the number or velocity of mobile mitochondria in *Dhc64C^{4-19} +/+ dSod1^{G85R}* MD neurons compared to the *Dhc64C^{4-19}*/+ phenotype, and no difference between *Dhc64c-RNAi/+* and *Dhc-64c-RNAi dSod1^{G85R}/+*

$dSod1^{G85R}$, indicating that the phenotype of one is not exacerbated by the other mutation, i.e., the two genes do not exhibit a genetic interaction (Fig 2C, Supp 3, Table 2). Targeting a different component which mediates dynein's cargo-binding ability, the Dynein intermediate chain (DIC), with the Dic^1 loss of function allele, also showed no phenotypic suppression or enhancement (Supp 4).

Similar tests using the *kinesin* (*Khc*) loss of function allele, Khc^{27-1}, that decreases the catalytic activity of Kinesin-1, showed that genetic combinations of $Khc^{27-1}/+$ with $dSod1^{G85R}$, either in a heterozygous or homozygous state, did not alter (suppress or enhance) the number or velocity of mobile mitochondria (Fig 2C, Supp 3). Together, these data indicate that it is unlikely that a defect in either of the two major microtubule motor proteins is responsible for the mitochondrial movement defect observed in $dSod1^{G85R}$.

Expression of *Miro*, a mitochondrial trafficking adaptor protein, is downregulated in $dSod1^{G85R}$

Cargos are linked to dynein and kinesin motors through adaptor proteins, such as Miro, a mitochondrial Rho GTPase, with calcium-sensing domains, with diverse functions in mitochondrial transport, as well as mitochondrial homeostasis, dynamics and Ca2+ homeostasis (Lee and Lu, 2014; Panchal & Tiwari 2021). In the spinal cords of human patients with ALS, the level of *Miro* expression has been reported to be reduced, as observed in the transgenic SOD1-G93A mouse ALS model (Smith 2017). We found that *Miro* levels are also reduced in $dSod1^{G85R}$ whole larvae (Fig 2E), prompting us to test if mitochondrial transport defects in $dSod1^{G85R}$ are ameliorated by overexpressing *Miro*. Overexpression of *Miro* alone (*UAS-Miro*) in wild type caused a reduction in the number of mobile mitochondria in MD axons (Figure 2F). But overexpression of *Miro* neither exacerbated, nor suppressed the $dSod1^{G85R}$ mobile mitochondrial defect, consistent with our findings that alterations in the axonal transport machinery is most likely not responsible for the reduction in mobile mitochondria in this ALS model.

Synaptic mitochondrial morphology preferentially disrupted in late 3rd instar $dSod1^{G85R}$ MD neurons

We examined the morphology of mitochondria in greater detail given that trafficking of mitochondria can be affected by their shape and that Miro is a known regulator of fission/fusion dynamics. A range of fifteen different structural elements were measured from 3D confocal reconstructions of mitochondria in the cell bodies and synaptic regions of MD neurons using the Mito-Analyzer Fiji Plugin (Chaudhry et al., 2020). First, to test the efficacy of Mito-Analyzer with our system, we analyzed mitochondria in MD neurons overexpressing *Miro*, known to alter mitochondrial morphology (Lee and Lu, 2014), and found the expected qualitative differences in structural parameters (Supp 5).

Mitochondria in the synaptic region of $dSod1^{G85R}$ MD neurons show a significant reduction in total and mean mitochondrial volume, total and mean surface area (SA), number of branches, branches per mitochondria, total and mean branch length, total branch length per mitochondria, number of branch junctions, branch junctions per mitochondria, branch end points per mitochondria, mean branch diameter, and a significant increase in the sphericity

of mitochondria (Fig 3A, Supp 6A). These data confirm our initial measurement of mitochondrial content which showed a reduction in *dSod1^{G85R}* synapses (Fig 1D). The more detailed analysis demonstrates that the decrease in synaptic mitochondrial content reflects a loss of networked mitochondria, with a gain in spherical mitochondria in *dSod1^{G85R}*. We found no morphological changes in mitochondria in MD da cell bodies in out MitoAnalyzer analysis (Fig 3B, Supp 6B), consistent with measures of total mitochondrial content showed (Fig 1D).

ALS is a progressive disease. We had previously identified the onset of locomotor defects associated with the *dSod1^{G85R}* model, within a 24hr window between early 3rd instar and wandering larvae (Sahin et al., 2017). We found no differences in morphological measures of mitochondria at the cell bodies or synaptic regions of *dSod1^{G85R}* and *dSod1^{WT}* MD neurons in early 3rd instar (Fig 3C-D, Supp 6 C,D), indicating changes in the mitochondrial network of *dSod1^{G85R}*-ALS correlates with the onset of a motor deficit.

Miro modifies mitochondrial morphology in *dSod1^{G85R}* MD neurons

In addition to Miro's function as an adaptor between mitochondrial and microtubule motor proteins, it has other important functions in mitochondrial biology. Miro interacts with mitochondrial proteins, Dynamic related protein 1 (Drp1), and Mitofusins 1/2 (Mfn1 and Mfn2), which regulate fission/fusion dynamics, respectively (Sheng et al., 2014). Given the decrease in *Miro* expression in *dSod1^{G85R}* (Fig 2E), and the shift is synaptic mitochondrial morphology from networked to spherical, we investigated the possibility that Miro's role in fission/fusion is impacted in *dSod1^{G85R}* mitochondria. We asked if an increase in *Miro* expression (*Miro-OE*) could restore defective mitochondrial morphology in *dSod1^{G85R}* (Fig 4A, Supp 7). Interestingly, *Miro* overexpression in *dSod1^{G85R}* heterozygotes (MD-Gal4>UAS-Miro, G85R/+ (MiroOE/G85R)) led to an increase in the volume of mitochondria in synapses, greater than that seen in *Miro* overexpression alone or in the *dSod1^{G85R}* homozygote (Fig 4A). The volume and branching defects in *dSod1^{G85R}* homozygotes also appear somewhat restored with the overexpression of *Miro*, although they do quite reach statistical significance.

In MD cell bodies, overexpression of *Miro* reduces the total volume and branching of mitochondria in a wild-type background (Fig 4B), however, this effect appears to be negated in *dSod1^{G85R}* homozygotes, suggesting that the ability of elevated Miro to reduce mitochondrial volume and branching in cell bodies is in some way blocked, or reduced, in *dSod1^{G85R}*. While Miro overexpression does not alone impact mitochondrial sphericity in cell bodies, a significant increase is seen in *dSod1^{G85R}* cell bodies, a phenotype also seen in synapses of *dSod1^{G85R}* homozygotes (Fig 4A,B, Table 2). Thus, while Miro's levels do not modify mitochondrial transport or subcellular localization, the morphological changes apparent in *dSod1^{G85R}* mitochondria (Fig 3, Suppl 6) could reflect a shift in fission/fusion dynamics due to a decrease in *Miro* expression levels (Fig 2E), defects that can be partially restored by experimentally increased Miro expression (Fig 4, Supp 7).

Fragmented *dSod1^{G85R}* mitochondria restored by reducing levels of the fission factor *Drp1*

Miro interacts with two other Drosophila proteins, Drp1 and Marf (mitochondrial assembly regulatory factor), an ortholog of Mfn1/2 to regulate fission and fusion, respectively. Since mitochondrial morphology and function are highly connected (Guo et al., 2018; Daum et. al., 2013; Nunnari and Suomalainen, 2012), i.e., mitochondrial fusion of healthy mitochondria is known to be upregulated in stressed conditions to maximize total OXPHOS in the cell. Fission, which generates new mitochondria, is also known to eliminate damaged mitochondria from the network of organelles (Youle and van der Bliek, 2013). Consistent with our findings for mitochondria at *dSod1^{G85R}* MD synapses, an increase in spherical or mitochondrial fragmentation due to increased fission is common in ALS patients and animal models alike (Altanbyek et al., 2016; Lopez-Gonzalez et al., 2016; Wijesekera and Leigh, 2009). Decreasing or inhibiting *Drp1* is known to ameliorate such mitochondrial defects (Choi et al., 2020; Joshi et al., 2018, Liu et al., 2013, Song et al., 2013). We tested if genetic manipulations the *Drosophila* ortholog of Drp1 would modify the highly fragmented synaptic mitochondria in *dSod1^{G85R}*. Animals homozygous for the *Drp1* null allele, *Drp1^{KG03815}*, are known to die early (1st instar stage) with elongated mitochondria (Rikhy et al., 2007). We found no change in sphericity of mitochondria at MD synapses in *Drp1^{KG03815}/+* heterozygotes, but a decrease in volume and branching was accompanied by a change in *Drp1* dosage in wild type animals (Fig 5A, C-F, Table 2, Supp 9). Interestingly, a reduction in *Drp1* in a *dSod1^{G85R}* background results in larger and more networked mitochondria, exhibiting a rescue of *dSod1^{G85R}* mitochondrial defects in synapses (Fig 5A-F', Table 2), and a reversal of the mild defects in sphericity in *dSod1^{G85R}* MD cell bodies (Fig 5B, C'-F'). Thus, mitochondrial fragmentation in *dSod1^{G85R}* can be reversed by reducing the function of the pro-fission factor *Drp1*. In a parallel set of experiments aimed at examining the impact of the profusion factor, *Marf*, we found animals homozygous for *dSod1^{G85R}* with a reduction in Marf by one dose (*Marf^8 dSod1^{G85R}/+ dSod1^{G85R}*) did not survive, thus a rescue could not be directly tested. No profound effects on mitochondrial morphology were observed in the *Marf^8 +/+ dSod1^{G85R}* transheterozygotes (Suppl 8, Table 2).

Mitophagy is elevated at the synapses but not in cell bodies of *dSod1^{G85R}* MD neurons

Our data thus far indicates that mitochondrial content is preferentially reduced at *dSod1^{G85R}* MD synapses with a higher degree of spherical mitochondria (Fig 1,3), an effect that can be rescued by increasing expression of *Miro* or decreasing the pro-fission factor *Drp1* (Fig 4,5). We questioned whether the altered morphology and abnormal distribution might result from an innate dysfunction of the mitochondria themselves, as trafficking of mitochondria does not appear to be significantly compromised. As a first measure for the presence of dysfunctional mitochondria, we assayed for their destruction. Damaged mitochondria are typically eliminated through mitophagy, a form of macro-autophagy, as an essential quality control mechanism for regulating mitochondrial homeostasis (Pickles et al., 2018). We made use of the *UAS-mito-QC* genetic reporter, a pH-sensitive fluorescent biosensor with an outer mitochondrial membrane (OMM)-localization signal fused to a dual mCherry-GFP fluorescent tag to assay mitochondrial turnover. In an acidic environment, typical of the lysosome or autophagosome, the GFP signal is quenched, while the mCherry signal is not, allowing us to visualize mitochondria that have been engulfed by lysosomes

(mitolysosomes) *in vivo* as red fluorescence (Lee et al., 2018; Garriga et al., 2020). The mito-QC biosensor was expressed in MD neurons (*MD>mitoQC*) and mitolysosomes were quantified as red fluorescing puncta (Fig 6). The MD synaptic regions of *dSod1^{G85R}* VNCs showed a higher number of red particles compared to controls (Fig 6A-B, E), with no change in mitolysosomes evident in da cell bodies (Fig 6C-E). An increase in mitolysosomes is indicative of higher levels of mitophagy which could account for the lower number of mitochondria in *dSod1^{G85R}* MD synapses, as well as being indicative of mitochondria whose function is compromised.

MD neurons of *dSod1^{G85R}* show compartment-specific changes in OXPHOS

As a measure of mitochondrial function, we assessed the oxidative state of mitochondria *in vivo*. The electron transport chain (ETC) functions in mitochondria to efficiently transport electrons through five protein complexes, creating an electrochemical proton gradient which drives the production of ATP, a process known as oxidative phosphorylation (OXPHOS). Redox couples act as regulators of OXPHOS, and their abundance and ratios are good indicators of the oxidative state of a cell. Since the oxidative state of different subcellular compartments is fluid, with an array of redox couples that may not be in equilibrium with one another, we tested two different redox pairs (Meyer and Dick, 2010). Redox-sensitive GFPs (ro-GFPs) contain a dithiol/disulfide switch on their surface that results in a redox-dependent shift in fluorescence that is not sensitive to pH (Dooley et al., 2004, Hanson et al., 2004). Glutathione:glutathione-disulfide (GSH:GSSG) is one of the most abundant redox couples in the cell (Schafer & Buettner, 2001) and thus, a valuable indicator of a cell's oxidative state. The fusion of ro-GFP to glutaredoxin (Grx1) allows for effective measures of the glutathione redox potential.

Along with other oxidants, glutathione peroxidases catalyze the reduction of H_2O_2 into less reactive H_2O. Although H_2O_2 is a typical byproduct of a healthy cell, unregulated levels of this reactive oxygen species (ROS) will harm the cell membrane and activate apoptosis (Opie, 2014). The fusion of ro-GFP to oxidant receptor peroxidase 1 (Orp1) enabled the production of a H_2O_2 sensor (Albrecht, et al., 2011). ro-GFP-Grx1 and ro-GFP-Orp1 transgenes with sequences localizing the sensor to the mitochondrial matrix (*mito-roGFP*) allows for tissue-specific expression and *in vivo* measurements of GSSG:GSH and H_2O_2 levels (Albrecht, et al., 2011). We expressed ro-GFP-Grx1 pan-neuronally using ELAV-Gal4 (Gramates et al., 2022) and found mitochondria showed lower levels of GSSG in the *dSod1^{G85R}* VNC, more specifically in the dorsal midline cells and the neuropil (Fig 7A-C). The effectiveness of the probe was demonstrated by treating *dSod1^{WT}* samples with the DTT reductant which showed the expected reduction (Fig 7C). To assess the redox state of mitochondria specifically in *dSod1^{G85R}* MD neurons, each mito-ro-GFP was driven by MD-Gal4. Both redox couples exhibited a significant reduction in mitochondria of MD cell bodies (Fig 7G), with a non-significant but trending decrease in GSSG:GSH and H_2O_2 levels in the mitochondria of MD synapses (Fig 7E). We also tested the redox couples in mitochondria of motor neurons (*OK6-Gal4>mito-ro-GFP)* in *dSod1^{G85R}* and found significant decreases in GSSG levels in motor neuron cell bodies (Supp 10). Together, these findings are indicative of a system-wide disruption of redox couples in *dSod1^{G85R}* neurons.

As stated above, the motor deficit associated with the *dSod1^{G85R}*-ALS model, first evident in the latter half of the 3rd instar period (Sahin et al., 2017), correlates with a change in mitochondrial morphology (Fig 3). Consistent with this progressive change in mitochondrial morphology and motor output, we found no significant differences in GSSG:GSH or H_2O_2 levels in MD neurons of early 3rd instar *dSod1^{G85R}* (Fig 7 I-K), followed by a significant reduction in older animals. Thus, as motor activity declines, we observe a change in mitochondrial morphology and in the oxidative state of neurons, an indication that the function of mitochondria is compromised.

Downregulation of ETC Complex subunits reverses ALS-associated mitochondrial defect

OXPHOS homeostasis is impacted by the proper function of ETC complexes. Disruptions in a single subunit of an ETC Complex can lead to morphological changes that result in mitochondrial turnover. We identified four ETC complex subunit genes in an RNA-seq analysis, whose expressions are elevated in *dSod1^{G85R}* larval brain isolates (Zhou et al., manuscript in prep). These genes include: NADH-dehydrogenase 51kDa subunit-like 1 (ND-51L1), involved in dehydrogenase and nucleotide binding activity of Complex I; succinate dehydrogenase subunit B (iron-sulfur)-like (SdhBL), a subunit of Complex II, predicted to enable Complex II activity; coenzyme Q8 (*Coq8*) also known as the chaperone, ubiquinone; and cytochrome c oxidase subunit 6A-like 2 (COX6AL2) of Complex IV. Increases in these Complex subunits are expected to increase the flux of electrons through the ETC, which in turn would produce more free radicals and ROS, and thus inflict higher levels of cellular damage. In this context, knocking down the level of specific Complex I, II or IV subunits is predicted to slow flux, and thus, reduce cellular damage. We tested this hypothesis that reducing the expression of each genes will slow ETC flux, regain OXPHOS homeostasis, and restore the abnormal morphology of mitochondria in *dSod1^{G85R}* to a WT state.

Each gene was individually knocked down first in *dSod1^{WT}* and then in *dSod1^{G85R}* MD neurons using an RNAi (Table 1). The abundance and structural parameters of mitochondria in synapse and cell bodies of *dSod1^{WT}* and *dSod1^{G85R}* MD neurons were assayed using 3D volumetric rendering of confocal images and the MitoAnalyzer for quantification (Fig 8, Supp 11). In wild type MD neurons, the knock down of ND-51L1 caused a significant increase in mitochondrial sphericity at synapses, with lower levels trending at cell bodies and no change in the total volume or branch number of mitochondria at synapses or cell bodies (Fig 8, Supp 11A). MD>SdhBL-RNAi did not affect mitochondrial morphology at synapses in wild type but caused a dramatic increase in the total volume and branching in MD cell bodies (Fig 8, Supp 11B). MD>*Coq8*-RNAi resulted in an increase in branching at cell bodies in wild type but had no effect on mitochondrial morphology at the synapse (Fig 8, Supp 11C). MD>*COX6AL2-RNAi* (*CG14077-RNAi*) had no effect on synaptic mitochondria in wild type but increased branching of mitochondria at the cell body (Fig 8, Supp 11D). Together, these data provide a clear demonstration that the manipulations of individual ETC Complex subunits can alter the morphology of mitochondrial networks in distinct neuronal compartments (Fig 8, Supp 11).

In a *dSod1*^{G85R} background, knocking down individual Complex I, II, and IV subunits, *ND-51L1, SdhBL,* and *COX6AL2*, respectively, resulted in a rescue, or restoration of defective mitochondrial morphologies at *dSod1*^{G85R} MD synapses to the wildtype state (Fig 8, Table 2). While its expression is elevated in *dSod1*^{G85R}, knocking down *Coq8*, a chaperone, did not reverse the majority of mitochondrial defects (Fig 8, Table 2).

Of particular interest, silencing *SdhBL* suppressed the defect in mitochondrial trafficking evident in *dSod1*^{G85R} MD axons, resulting in an increase the number of mobile mitochondria (Supp 12A-E). It has been shown that ETC Complexes exhibit compensatory actions, wherein the activity of one Complex is upregulated if another is downregulated in an attempt to restore ETC-homeostasis, an essential process for mitochondrial survival (Weinrich et al., 2019). We, too, found evidence of the compensatory behavior of ETC Complexes, when silencing one subunit, SdhBL, we found an upregulation of another, ND-51L1 (Sup 12F). Thus, taken together our data demonstrate that elevated levels of *ND-51L1, SdhBL,* and *COX6AL2* transcripts correlate with abnormal mitochondrial properties in *dSod1*^{G85R} animals, and in each case, the downregulation of each gene's expression reverses defects in mitochondria associated with the ALS mutation.

Discussion

In this study, we sought to determine the nature of mitochondrial defects associated with the neurodegenerative disease ALS, using a knock-in SOD1 model in *Drosophila* where live-imaging and *in vivo* measurements of mitochondrial morphology and function allows for analysis within subcellular compartments in a cell-type specific manner, in the context of the intact motor circuit. We focused our study on sensory neurons, having demonstrated previously that functional defects in sensory feedback precedes degeneration of motor neurons and coincides with a decline in locomotor activity in the *dSod1*^{G85R} knock-in ALS model (Held et al., 2019; Sahin et al., 2017). The *dSod1*^{G85R}-ALS animals exhibit reduced numbers of mobile mitochondria in MD sensory axons, lower mitochondrial content at synapses with significant morphological defects, and little to no change in the mitochondrial pool present in cell bodies (Fig 1, 3, 9A-D). We did not detect any obvious disruptions in transport machinery that could account for difference in synaptic vs cell body mitochondrial content (Fig 2, 9E), but instead found higher levels of mitophagy in synaptic regions (Fig 6, 9C). Studies in other models of ALS, such as transfected primary cultures of embryonic rat motor neurons have reported defects in axonal transport albeit how specific types of cargo, i.e., mitochondria, vesicles, or other cargo, respond is different between neuronal cell types, mutants, and animal models of ALS (Baldwin et al., 2016; De Vos et al., 2007; Moller et al., 2017; Morotz et al., 2012). For example, the transport of neuropeptide Y-containing vesicles, but not mitochondria, is affected when human TDP43 is overexpressed in *Drosophila* motor neurons. In contrast, the loss of *TBPH*, a *Drosophila* TDP43 ortholog, shows compromised axonal transport of mitochondria, but not of vesicles, a similar finding when *FUS* or G$_4$C$_2$-36X repeats are overexpressed (Baldwin et al., 2016). In our knock-in *dSod1*^{G85R} ALS model, we, too, found that the transport of all cargos is not affected, as lysosomal and vesicular transport is unchanged in *dSod1*^{G85R} MD sensory neurons (Fig 2, 9B).

Some transport studies have detected a preferential decrease in anterograde, or retrograde transport, although consistent with our findings they, too, have found that a defect in the microtubule transport-machinery is unlikely to give rise to the abnormal distribution of mitochondria (Moller et al., 2017, Magrane et al., 2013). We did not observe a preference in directional movement, but instead found the mobile pool of mitochondria in $dSod1^{G85R}$ sensory axons, is preferentially reduced, while the stationary pool is not (Fig 1, 9A). Stationary mitochondria are known to be anchored along axons in areas of high ATP demand, such as at spots of active translation in sensory neurons (Spillane et al., 2013). Local translation of mRNAs is upregulated during neuronal damage or during homeostatic changes that promote axon growth, regeneration, branching, synaptic formations, and protein transport (Nagano and Araki 2021; Holt et al., 2019). It is indeed possible that there may be a need In $dSod1^{G85R}$ sensory neurons for increased axonal translation requiring ATP production by anchored mitochondria, and thus, the stationary pool of mitochondria is maintained. In fact, our observation that the length of dendritic branches of ddaE MD neurons is increased in $dSod1^{G85R}$ (Fig 9D, Supp 1), is consistent with a need for local energy production perhaps to fuel translation necessary for the promotion of neuronal elongation, a consideration that needs further exploration.

Interestingly, *in vivo* biosensors revealed shifts in the oxidative state of neurons in $dSod1^{G85R}$, indicative of compromised mitochondrial function (Fig 7). Consistent with an alleviation of the effects of dysfunctional mitochondria, downregulation of subunits in Complex I, II or IV of the ETC restored mitochondrial morphology and SdhBL of Complex II partially rescued the reduction in mobile mitochondria typical of $dSod1^{G85R}$ sensory axons (Fig 8).

Interestingly, the $dSod1^{G85R}$ knock-in model exhibits mitochondrial morphology and function that differ between distinct subcellular domains within MD neurons, whole-organelle structural differences at synapses, with no significant morphological changes in mitochondria that reside in MD cell bodies (Fig 3, 9A,B). The morphological changes at the synapse can be rescued by reducing the dosage of the fission factor *Drp1* (Fig 5) suggesting that an imbalance in fission-fusion dynamics could be responsible for the $dSod1^{G85R}$ phenotype.

Although *Marf*^{B} and $dSod1^{G85R}$ did not exhibit a genetic interaction, as *Marf*^{B}/+; $dSod1^{G85R}$/+ mitochondrial morphology at synaptic regions was unchanged (Supp 6, 9B,C), there was noticeable clustering of mitochondria in cell bodies. Such an increase in mitochondrial clustering is prominently observed in studies of Charcot-Marie-Tooth Disease when expressing Mitofusin 2 (MFN2, the ortholog of *Marf*) mutants in cultured neurons (Baloh, et al., 2007). This study also showed a decreased in mobile mitochondria in axons of MFN2 mutants. Since *Marf* is known to directly interact with OMM components like *Miro* (Lee et al., 2016), it is not surprising that genetically manipulating these factors results in similar mitochondrial defects. Given that we see a genetic interaction between $dSod1^{G85R}$ and *Miro*, it may be that knocking down the function of *Marf* results in a disruption of *Miro* function, thereby enhancing the abnormal morphological changes evident in $dSod1^{G85R}$ mitochondria.

Defects in mitochondrial function may stem from improper fluctuations in their oxidative state which is regulated by the ETC. Our data indicates that mitochondrial defects in an ALS model can be rescued by genetically manipulating subunits of ETC complex I, II, and IV (Fig 8, 9F). Indeed, drugs that target the ETC and its products have been tested in animal models of NDs to ameliorate mitochondrial dysfunction. MitoQ, a mitochondria-specific antioxidant, shown to reduce ROS, preserves mitochondrial function in models of Alzheimer's (McManus et al., 2011), Parkinson's (Solesio et al., 2013, Ghosh et al., 2010), ALS (Miquel et al., 2014), and other NDs (Dhanasekaran et al., 2004; Jauslin et al., 2003). At present difficulties in the delivery, targeting, and adverse effects of small molecules such as MitoQ, have to date impacted its clinical value (Xu et al., 2022). In another case, while Coenzyme Q10, a scavenger drug that targets ROS produced by the ETC, has shown beneficial effects in some models of ALS (Matthews et al., 1998), it is not proven effective in the clinical setting (Kaufmann et al., 2009). Interestingly, while expression of the Coq8 chaperone is altered in the $dSod1^{G85R}$-ALS model, we found *in vivo* manipulation of Coq8 did not ameliorate mitochondrial defects, consistent with the clinical findings of Coenzyme Q10. The fact that common molecular pathways are revealed by both *Drosophila* and mammalian models is promising for the use of such models in efforts to identify more targets that provide new avenues for the development of effective therapies. It is also important to consider that although ETC complexes in mammals and yeast are known to form supercomplexes, to provide more efficient electron transfer (Cogliati et al., 2021), a structure not seen in *Drosophila* mitochondria (Shimada et al., 2018), our analysis has revealed that manipulations of ETC components can have clear restorative effects in the context of neurodegeneration. These findings also support the proposal that mechanisms are in place in the mitochondrial membrane of *Drosophila* that negate the need for supercomplexes to enable efficient electron transfer (Shimada et al., 2018).

An upregulation of mitochondrial turnover via mitophagy, that can stem from disruptions in mitochondrial homeostasis, has been documented in spinal cord motor neurons of ALS patients (Sasaki, 2011). We, too, see an increase in mitochondrial turnover in the $dSod1^{G85R}$-knock-in ALS model, accompanied by a decrease in compartment-specific mitochondrial content (Fig 6, 9C). Pan-neuronal expression of a mitochondria-specific redox-sensitive GFP biosensor showed a general disruption in OXPHOS in $dSod1^{G85R}$ (Fig 7A-C) indicating a reduction in mitochondrial function, and consistent with the elevation of mitophagy which would eliminate defective mitochondria. Both motor neuron cell bodies and the neuropil, sites of sensory synaptic connections show a reduction in mito-ro-GFP-Grx1 signal, an indication of GSSG:GSH level (Fig 7A-C). Neuron-specific analysis showed that at the point in disease progression examined, the heightened level of mitophagy is particularly evident in the synaptic regions of MD sensory neurons (Fig 7D-G), where dramatic changes in mitochondrial morphology are apparent (Fig 3A-B'). At this time, mitochondria-specific redox-sensitive GFP (mito-ro-GFP) biosensors showed a significant decrease in GSSG:GSH and H_2O_2 levels in cell bodies, with a trending, albeit not significant, decrease in MD synapses (Fig 7D-G, 9F), suggesting that while alterations in metabolic flux are detected in the cell body, a shift in metabolic dysfunction due to elevated GSSG:GSH or H_2O_2 levels may not be resolved because mitochondria harboring those redox changes have already been eliminated. Assessments of both mitochondrial

morphology and redox couples at a slightly earlier time showed no differences between the knock-in ALS model and wild type animals (Fig 3 C-D', 7H-K). As such, within the later time window which is characterized by electrophysiological changes in sensory function and compromised locomotor activity, the redox changes observed in synapses may have reached a critical threshold but not reached in the cell bodies to warrant significant turnover of resident mitochondria. In addition, or alternatively, defective mitochondria are sent from the cell bodies to the synapses where demands on their function may be more profound, perhaps coupled with a defect in fission/fusion dynamics, and thus, there they are destroyed.

Decreases in mitochondrial GSSG:GSH levels are indicative of an increase in reduced glutathione levels, which act on ROS such as H_2O_2 (Armstrong et al., 2002, Fernandez-Checa et al., 1997). Thus, a decrease in GSSG:GSH would predict an increase in H_2O_2 levels, and indeed abnormally high levels of have been observed in ALS patients' blood (Woolsey, 2008). However, an upregulation of H_2O_2 would be accompanied by an upregulation of scavenging factors, such as thioredoxins, and the balance in production- and scavenging- of ROS would result as an irregular flux and manifest as increased H_2O_2 flux (Miguel Antonio Aon et al., 2012). It is also possible that the loss of enzymatic Sod1 activity in the intermembrane mitochondrial space (IMS) is associated with reduced dismutation of superoxide anions and thus, lower H_2O_2, unrelated to the low levels of GSSG (Goldsteins et al., 2008). Our findings indicate a change in metabolic flux associated with $dSod1^{G85R}$ mitochondria that likely reflects an innate dysfunction.

Our studies presented here focused on sensory neurons based on previous *in vivo* findings that these neurons exhibit profound dysfunction prior to motor neuron defects (Held et al., 2019), that ALS-associated motor dysfunction and death could be suppressed by genetic manipulations targeting only sensory neurons, and the availability of reagents that provided sufficient resolution of mitochondria *in vivo*. However, in addition to these studies, we were able to assay the status of mitochondria in motor neurons in some contexts of the $dSod1^{G85R}$-knock-in animals, and documented alterations in mitochondrial content, morphology, and redox couples. Future *in vivo* studies of mitochondrial biology in motor neurons are warranted with more refined drivers. In addition, comparative studies at higher resolution such as serial block-face electron microscopy could provide a higher resolution 3D reconstruction of the mitochondrial ultrastructure in all types of neurons. Such analyses would provide more detailed information about the composition and surface area of the cristae structure in $dSod1^{G85R}$, an essential cellular compartment for maintaining proper mitochondrial homeostasis (Cogliati et al., 2016), especially given the observed impact of ETC complexes which reside within the cristae. Such high-resolution studies could extend our understanding between changes in mitochondrial ultrastructure and OXPHOS in the $dSod1^{G85R}$ ALS model.

Taken together, our results identify compartment-specific alterations in mitochondrial number, morphology, mitophagy, and OXPHOS in MD sensory neurons of a SOD1-knock-in model of ALS, $dSod1^{G85R}$. The role of sensory neurons in ALS is now becoming more appreciated, with such research providing evidence of the value of such studies. Our data highlight that abnormal mitochondrial transport, which is common in many NDs, may not always stem from defects in the trafficking machinery, but instead from innate mitochondrial

Author Manuscript

dysfunction, an important consideration in discerning mechanisms of pathogenesis. We demonstrate that defects in mitochondrial morphology can be restored to wild type levels by altered expression of specific genes encoding OXPHOS subunits, as well as by shifting mitochondrial fission/fusion dynamics. While advancing our understanding of the specific mitochondrial defects associated with ALS mutations, these findings have identified specific targets for future exploration of therapeutic potential, a valuable contribution to combating ALS.

Supplementary Material

Refer to Web version on PubMed Central for supplementary material.

Financial support:

Abbreviations:

ALS	amyotrophic lateral sclerosis
ND	neurodegenerative disease
ETC	electron transport chain
ROS	reactive oxygen species
MD	multidendritic

References

Albrecht SC, Barata AG, Großhans J, Teleman AA, & Dick TP (2011). In Vivo Mapping of Hydrogen Peroxide and Oxidized Glutathione Reveals Chemical and Regional Specificity of Redox Homeostasis. Cell Metabolism, 14(6), 819–829. 10.1016/j.cmet.2011.10.010 [PubMed: 22100409]

Altanbyek V, Cha S-J, Kang G-U, Im DS, Lee S, Kim H-J, & Kim K (2016). Imbalance of mitochondrial dynamics in Drosophila models of amyotrophic lateral sclerosis. Biochemical and Biophysical Research Communications, 481(3–4), 259–264. 10.1016/j.bbrc.2016.10.134 [PubMed: 27810362]

Amylyx Pharmaceuticals Inc. (2021). Evaluation of the Safety, Tolerability, Efficacy and Activity of AMX0035, a Fixed Combination of Phenylbutyrate (PB) and Tauroursodeoxycholic Acid (TUDCA), for the Treatment of ALS (Clinical Trial Registration No. NCT03127514). clinicaltrials.gov. https://clinicaltrials.gov/ct2/show/NCT03127514

Anoar S, Woodling NS, & Niccoli T (2021). Mitochondria Dysfunction in Frontotemporal Dementia/ Amyotrophic Lateral Sclerosis: Lessons From Drosophila Models. Frontiers in Neuroscience, 15, 786076. 10.3389/fnins.2021.786076 [PubMed: 34899176]

Aon MA, Stanley BA, Sivakumaran V, Kembro JM, O'Rourke B, Paolocci N, & Cortassa S (2012). Glutathione/thioredoxin systems modulate mitochondrial H2O2 emission: An experimental-computational study. Journal of General Physiology, 139(6), 479–491. 10.1085/jgp.201210772 [PubMed: 22585969]

Armstrong JS, Steinauer KK, Hornung B, Irish JM, Lecane P, Birrell GW, Peehl DM, & Knox SJ (2002). Role of glutathione depletion and reactive oxygen species generation in apoptotic

signaling in a human B lymphoma cell line. Cell Death & Differentiation, 9(3), 252–263. 10.1038/sj.cdd.4400959 [PubMed: 11859408]

Baldwin KR, Godena VK, Hewitt VL, & Whitworth AJ (2016). Axonal transport defects are a common phenotype in Drosophila models of ALS. Human Molecular Genetics, ddw105. 10.1093/hmg/ddw105

Baloh RH, Schmidt RE, Pestronk A, & Milbrandt J (2007). Altered Axonal Mitochondrial Transport in the Pathogenesis of Charcot-Marie-Tooth Disease from Mitofusin 2 Mutations. Journal of Neuroscience, 27(2), 422–430. 10.1523/JNEUROSCI.4798-06.2007 [PubMed: 17215403]

Brotherton TE, Li Y, & Glass JD (2013). Cellular toxicity of mutant SOD1 protein is linked to an easily soluble, non-aggregated form in vitro. Neurobiology of Disease, 49, 49–56. 10.1016/j.nbd.2012.08.010 [PubMed: 22926189]

Brown RH, & Al-Chalabi A (2017). Amyotrophic Lateral Sclerosis. New England Journal of Medicine, 377(2), 162–172. 10.1056/NEJMra1603471 [PubMed: 28700839]

Cassina P, Miquel E, Martínez-Palma L, & Cassina A (2021). Glial Metabolic Reprogramming in Amyotrophic Lateral Sclerosis. Neuroimmunomodulation, 28(4), 204–212. 10.1159/000516926 [PubMed: 34175843]

Chai A, & Pennetta G (2015). Insights into ALS pathomechanisms: From flies to humans. Fly, 9(2), 91–98. 10.1080/19336934.2015.1114694 [PubMed: 26594942]

Chaudhry A, Shi R, & Luciani DS (2020). A pipeline for multidimensional confocal analysis of mitochondrial morphology, function, and dynamics in pancreatic β-cells. American Journal of Physiology-Endocrinology and Metabolism, 318(2), E87–E101. 10.1152/ajpendo.00457.2019 [PubMed: 31846372]

Chen S, Sayana P, Zhang X, & Le W (2013). Genetics of amyotrophic lateral sclerosis: An update. Molecular Neurodegeneration, 8(1), 28. 10.1186/1750-1326-8-28 [PubMed: 23941283]

Choi SY, Lee J-H, Chung A-Y, Jo Y, Shin J, Park H-C, Kim H, Lopez-Gonzalez R, Ryu JR, & Sun W (2020). Prevention of mitochondrial impairment by inhibition of protein phosphatase 1 activity in amyotrophic lateral sclerosis. Cell Death & Disease, 11(10), 888. 10.1038/s41419-020-03102-8 [PubMed: 33087694]

Cogliati S, Cabrera-Alarcón JL, & Enriquez JA (2021). Regulation and functional role of the electron transport chain supercomplexes. Biochemical Society Transactions, 49(6), 2655–2668. 10.1042/BST20210460 [PubMed: 34747989]

Cogliati S, Enriquez JA, & Scorrano L (2016). Mitochondrial Cristae: Where Beauty Meets Functionality. Trends in Biochemical Sciences, 41(3), 261–273. 10.1016/j.tibs.2016.01.001 [PubMed: 26857402]

Cooke MS, Evans MD, Dizdaroglu M, & Lunec J (2003). Oxidative DNA damage: Mechanisms, mutation, and disease. The FASEB Journal, 17(10), 1195–1214. 10.1096/fj.02-0752rev [PubMed: 12832285]

Daum B, Walter A, Horst A, Osiewacz HD, & Kühlbrandt W (2013). Age-dependent dissociation of ATP synthase dimers and loss of inner-membrane cristae in mitochondria. Proceedings of the National Academy of Sciences, 110(38), 15301–15306. 10.1073/pnas.1305462110

De Vos KJ, Chapman AL, Tennant ME, Manser C, Tudor EL, Lau K-F, Brownlees J, Ackerley S, Shaw PJ, McLoughlin DM, Shaw CE, Leigh PN, Miller CCJ, & Grierson AJ (2007a). Familial amyotrophic lateral sclerosis-linked SOD1 mutants perturb fast axonal transport to reduce axonal mitochondria content. Human Molecular Genetics, 16(22), 2720–2728. 10.1093/hmg/ddm226 [PubMed: 17725983]

Dhanasekaran A, Kotamraju S, Kalivendi SV, Matsunaga T, Shang T, Keszler A, Joseph J, & Kalyanaraman B (2004). Supplementation of Endothelial Cells with Mitochondria-targeted Antioxidants Inhibit Peroxide-induced Mitochondrial Iron Uptake, Oxidative Damage, and Apoptosis. Journal of Biological Chemistry, 279(36), 37575–37587. 10.1074/jbc.M404003200 [PubMed: 15220329]

Dooley CT, Dore TM, Hanson GT, Jackson WC, Remington SJ, & Tsien RY (2004). Imaging Dynamic Redox Changes in Mammalian Cells with Green Fluorescent Protein Indicators *. Journal of Biological Chemistry, 279(21), 22284–22293. 10.1074/jbc.M312847200 [PubMed: 14985369]

Duffy JB (2002). GAL4 system in drosophila: A fly geneticist's swiss army knife. Genesis, 34(1–2), 1–15. 10.1002/gene.10150 [PubMed: 12324939]

Fernandez-Checa JC, Kaplowitz N, Garcia-Ruiz C, Colell A, Miranda M, Mari M, Ardite E, & Morales A (1997). GSH transport in mitochondria: Defense against TNF-induced oxidative stress and alcohol-induced defect. American Journal of Physiology-Gastrointestinal and Liver Physiology, 273(1), G7–G17. 10.1152/ajpgi.1997.273.1.G7

Gale Encyclopedia of Medicine. (2008). Bulbar muscles. TheFreeDictionary.Com. https://medical-dictionary.thefreedictionary.com/Bulbar+muscles

Ghosh A, Chandran K, Kalivendi SV, Joseph J, Antholine WE, Hillard CJ, Kanthasamy A, Kanthasamy A, & Kalyanaraman B (2010). Neuroprotection by a mitochondria-targeted drug in a Parkinson's disease model. Free Radical Biology and Medicine, 49(11), 1674–1684. 10.1016/j.freeradbiomed.2010.08.028 [PubMed: 20828611]

Gill C, Phelan JP, Hatzipetros T, Kidd JD, Tassinari VR, Levine B, Wang MZ, Moreno A, Thompson K, Maier M, Grimm J, Gill A, Vierira FG (2019) SOD1-positive aggregate accumulation in the CNS predicts slower disease progression and increased longevity in mutant SOD1 mouse model of ALS. Science Reports 9(1), 6724 10.1038/s41598-019-43164-z

Glancy B, Kim Y, Katti P, & Willingham TB (2020). The Functional Impact of Mitochondrial Structure Across Subcellular Scales. Frontiers in Physiology, 11, 541040. 10.3389/fphys.2020.541040 [PubMed: 33262702]

Goldsteins G, Keksa-Goldsteine V, Ahtoniemi T, Jaronen M, Arens E, Åkerman K, Chan PH, & Koistinaho J (2008). Deleterious Role of Superoxide Dismutase in the Mitochondrial Intermembrane Space. Journal of Biological Chemistry, 283(13), 8446–8452. 10.1074/jbc.M706111200 [PubMed: 18171673]

Gramates LS, Agapite J, Attrill H, Calvi BR, Crosby MA, dos Santos G, Goodman JL, Goutte-Gattat D, Jenkins VK, Kaufman T, Larkin A, Matthews BB, Millburn G, Strelets VB, the FlyBase Consortium, Perrimon N, Gelbart SR, Agapite J, Broll K, … Lovato T (2022). FlyBase: A guided tour of highlighted features. Genetics, 220(4), iyac035. 10.1093/genetics/iyac035 [PubMed: 35266522]

Guo R, Gu J, Zong S, Wu M, & Yang M (2018). Structure and mechanism of mitochondrial electron transport chain. Biomedical Journal, 41(1), 9–20. 10.1016/j.bj.2017.12.001 [PubMed: 29673555]

Hanson GT, Aggeler R, Oglesbee D, Cannon M, Capaldi RA, Tsien RY, & Remington SJ (2004). Investigating Mitochondrial Redox Potential with Redox-sensitive Green Fluorescent Protein Indicators *. Journal of Biological Chemistry, 279(13), 13044–13053. 10.1074/jbc.M312846200 [PubMed: 14722062]

Hardiman O, Al-Chalabi A, Chio A, Corr EM, Logroscino G, Robberecht W, Shaw PJ, Simmons Z, & van den Berg LH (2017). Amyotrophic lateral sclerosis. Nature Reviews Disease Primers, 3(1), 17071. 10.1038/nrdp.2017.71

Held A, Major P, Sahin A, Reenan RA, Lipscombe D, & Wharton KA (2019). Circuit Dysfunction in SOD1-ALS Model First Detected in Sensory Feedback Prior to Motor Neuron Degeneration Is Alleviated by BMP Signaling. The Journal of Neuroscience, 39(12), 2347–2364. 10.1523/JNEUROSCI.1771-18.2019 [PubMed: 30659087]

Hink HU, Santanam N, Dikalov S, McCann L, Nguyen AD, Parthasarathy S, Harrison DG, & Fukai T (2002). Peroxidase Properties of Extracellular Superoxide Dismutase: Role of Uric Acid in Modulating In Vivo Activity. Arteriosclerosis, Thrombosis, and Vascular Biology, 22(9), 1402–1408. 10.1161/01.ATV.0000027524.86752.02 [PubMed: 12231557]

Holt CE, Martin KC, & Schuman EM (2019). Local translation in neurons: Visualization and function. Nature Structural & Molecular Biology, 26(7), 557–566. 10.1038/s41594-019-0263-5

Hughes CL, & Thomas JB (2007). A sensory feedback circuit coordinates muscle activity in Drosophila. Molecular and Cellular Neuroscience, 35(2), 383–396. 10.1016/j.mcn.2007.04.001 [PubMed: 17498969]

Ilieva HS, Yamanaka K, Malkmus S, Kakinohana O, Yaksh T, Marsala M, & Cleveland DW (2008). Mutant dynein (Loa) triggers proprioceptive axon loss that extends survival only in the SOD1 ALS model with highest motor neuron death. Proceedings of the National Academy of Sciences, 105(34), 12599–12604. 10.1073/pnas.0805422105

Jauslin ML, Meier T, Smith RAJ, & Murphy PM (2003). Mitochondria-targeted antioxidants protect Friedreich Ataxia fibroblasts from endogenous oxidative stress more effectively than untargeted antioxidants. The FASEB Journal, 17(13), 1–10. 10.1096/fj.03-0240fje [PubMed: 12522106]

Joshi AU, Saw NL, Vogel H, Cunnigham AD, Shamloo M, & Mochly-Rosen D (2018). Inhibition of Drp1/Fis1 interaction slows progression of amyotrophic lateral sclerosis. EMBO Molecular Medicine, 10(3). 10.15252/emmm.201708166

Kaufmann P, Thompson JLP, Levy G, Buchsbaum R, Shefner J, Krivickas LS, Katz J, Rollins Y, Barohn RJ, Jackson CE, Tiryaki E, Lomen-Hoerth C, Armon C, Tandan R, Rudnicki SA, Rezania K, Sufit R, Pestronk A, Novella SP, … QALS Study Group. (2009). Phase II trial of CoQ10 for ALS finds insufficient evidence to justify phase III. Annals of Neurology, 66(2), 235–244. 10.1002/ana.21743 [PubMed: 19743457]

Kirby J, Al Sultan A, Waller R, & Heath P (2016). The genetics of amyotrophic lateral sclerosis: Current insights. Degenerative Neurological and Neuromuscular Disease, 49. 10.2147/DNND.S84956

Kohsaka H, Okusawa S, Itakura Y, Fushiki A, & Nose A (2012). Development of larval motor circuits in Drosophila. Development, Growth & Differentiation, 54(3), 408–419. 10.1111/j.1440-169X.2012.01347.x

Laudati G, Mascolo L, Guida N, Sirabella R, Pizzorusso V, Bruzzaniti S, Serani A, Di Renzo G, Canzoniero LMT, & Formisano L (2019). Resveratrol treatment reduces the vulnerability of SH-SY5Y cells and cortical neurons overexpressing SOD1-G93A to Thimerosal toxicity through SIRT1/DREAM/PDYN pathway. Neurotoxicology, 71, 6–15. 10.1016/j.neuro.2018.11.009 [PubMed: 30503815]

Lee JJ, Sanchez-Martinez A, Zarate AM, Benincá C, Mayor U, Clague MJ, & Whitworth AJ (2018). Basal mitophagy is widespread in Drosophila but minimally affected by loss of Pink1 or parkin. Journal of Cell Biology, 217(5), 1613–1622. 10.1083/jcb.201801044 [PubMed: 29500189]

Lee K-S, & Lu B (2014). The myriad roles of Miro in the nervous system: Axonal transport of mitochondria and beyond. Frontiers in Cellular Neuroscience, 8. 10.3389/fncel.2014.00330

Lee S, Lee K-S, Huh S, Liu S, Lee D-Y, Hong SH, Yu K, & Lu B (2016). Polo Kinase Phosphorylates Miro to Control ER-Mitochondria Contact Sites and Mitochondrial Ca 2+ Homeostasis in Neural Stem Cell Development. Developmental Cell, 37(2), 174–189. 10.1016/j.devcel.2016.03.023 [PubMed: 27093086]

Liu W, Yamashita T, Tian F, Morimoto N, Ikeda Y, Deguchi K, & Abe K (2013). Mitochondrial Fusion and Fission Proteins Expression Dynamically Change in a Murine Model of Amyotrophic Lateral Sclerosis. Current Neurovascular Research, 10(3), 222–230. 10.2174/15672026113109990060 [PubMed: 23713734]

Liu L, MacKenzie KR, Putluri N, Maleti -Savati M, & Bellen HJ (2017). The Glia-Neuron Lactate Shuttle and Elevated ROS Promote Lipid Synthesis in Neurons and Lipid Droplet Accumulation in Glia via APOE/D. Cell Metabolism, 26(5), 719–737.e6. 10.1016/j.cmet.2017.08.024 [PubMed: 28965825]

Lopez-Gonzalez R, Lu Y, Gendron TF, Karydas A, Tran H, Yang D, Petrucelli L, Miller BL, Almeida S, & Gao F-B (2016). Poly(GR) in C9ORF72 -Related ALS/FTD Compromises Mitochondrial Function and Increases Oxidative Stress and DNA Damage in iPSC-Derived Motor Neurons. Neuron, 92(2), 383–391. 10.1016/j.neuron.2016.09.015 [PubMed: 27720481]

Magrane J, Sahawneh MA, Przedborski S, Estevez AG, & Manfredi G (2012). Mitochondrial Dynamics and Bioenergetic Dysfunction Is Associated with Synaptic Alterations in Mutant SOD1 Motor Neurons. Journal of Neuroscience, 32(1), 229–242. 10.1523/JNEUROSCI.1233-11.2012 [PubMed: 22219285]

Mandal A, & Drerup CM (2019). Axonal Transport and Mitochondrial Function in Neurons. Frontiers in Cellular Neuroscience, 13, 373. 10.3389/fncel.2019.00373 [PubMed: 31447650]

Martin LJ (2010). Olesoxime, a cholesterol-like neuroprotectant for the potential treatment of amyotrophic lateral sclerosis. IDrugs: The Investigational Drugs Journal, 13(8), 568–580. [PubMed: 20721828]

Martin M, Iyadurai SJ, Gassman A, Gindhart JG, Hays TS, & Saxton WM (1999). Cytoplasmic Dynein, the Dynactin Complex, and Kinesin Are Interdependent and Essential for Fast Axonal

Transport. Molecular Biology of the Cell, 10(11), 3717–3728. 10.1091/mbc.10.11.3717 [PubMed: 10564267]

Masrori P, & Van Damme P (2020). Amyotrophic lateral sclerosis: A clinical review. European Journal of Neurology, 27(10), 1918–1929. 10.1111/ene.14393 [PubMed: 32526057]

Matthews RT, Yang L, Browne S, Baik M, & Beal MF (1998). Coenzyme Q $_{10}$ administration increases brain mitochondrial concentrations and exerts neuroprotective effects. Proceedings of the National Academy of Sciences, 95(15), 8892–8897. 10.1073/pnas.95.15.8892

McManus MJ, Murphy MP, & Franklin JL (2011). The Mitochondria-Targeted Antioxidant MitoQ Prevents Loss of Spatial Memory Retention and Early Neuropathology in a Transgenic Mouse Model of Alzheimer's Disease. Journal of Neuroscience, 31(44), 15703–15715. 10.1523/JNEUROSCI.0552-11.2011 [PubMed: 22049413]

Meyer AJ, & Dick TP (2010). Fluorescent Protein-Based Redox Probes. Antioxidants & Redox Signaling, 13(5), 621–650. 10.1089/ars.2009.2948 [PubMed: 20088706]

Miquel E, Cassina A, Martínez-Palma L, Souza JM, Bolatto C, Rodríguez-Bottero S, Logan A, Smith RAJ, Murphy MP, Barbeito L, Radi R, & Cassina P (2014). Neuroprotective effects of the mitochondria-targeted antioxidant MitoQ in a model of inherited amyotrophic lateral sclerosis. Free Radical Biology and Medicine, 70, 204–213. 10.1016/j.freeradbiomed.2014.02.019 [PubMed: 24582549]

Mishra P, & Chan DC (2014). Mitochondrial dynamics and inheritance during cell division, development and disease. Nature Reviews Molecular Cell Biology, 15(10), 634–646. 10.1038/nrm3877 [PubMed: 25237825]

Moller A, Bauer CS, Cohen RN, Webster CP, & De Vos KJ (2017). Amyotrophic lateral sclerosis-associated mutant SOD1 inhibits anterograde axonal transport of mitochondria by reducing Miro1 levels. Human Molecular Genetics, 26(23), 4668–4679. 10.1093/hmg/ddx348 [PubMed: 28973175]

Montava-Garriga L, Singh F, Ball G, & Ganley IG (2020). Semi-automated quantitation of mitophagy in cells and tissues. Mechanisms of Ageing and Development, 185, 111196. 10.1016/j.mad.2019.111196 [PubMed: 31843465]

Morotz GM, De Vos KJ, Vagnoni A, Ackerley S, Shaw CE, & Miller CCJ (2012). Amyotrophic lateral sclerosis-associated mutant VAPBP56S perturbs calcium homeostasis to disrupt axonal transport of mitochondria. Human Molecular Genetics, 21(9), 1979–1988. 10.1093/hmg/dds011 [PubMed: 22258555]

Muller FL, Song W, Liu Y, Chaudhuri A, Pieke-Dahl S, Strong R, Huang T-T, Epstein CJ, Roberts LJ, Csete M, Faulkner JA, & Van Remmen H (2006). Absence of CuZn superoxide dismutase leads to elevated oxidative stress and acceleration of age-dependent skeletal muscle atrophy. Free Radical Biology and Medicine, 40(11), 1993–2004. 10.1016/j.freeradbiomed.2006.01.036 [PubMed: 16716900]

Nagano S, & Araki T (2021). Axonal Transport and Local Translation of mRNA in Neurodegenerative Diseases. Frontiers in Molecular Neuroscience, 14, 697973. 10.3389/fnmol.2021.697973 [PubMed: 34194300]

Nunnari J, & Suomalainen A (2012). Mitochondria: In Sickness and in Health. Cell, 148(6), 1145–1159. 10.1016/j.cell.2012.02.035 [PubMed: 22424226]

Obrador E, Salvador R, López-Blanch R, Jihad-Jebbar A, Vallés SL, & Estrela JM (2020). Oxidative Stress, Neuroinflammation and Mitochondria in the Pathophysiology of Amyotrophic Lateral Sclerosis. Antioxidants, 9(9), 901. 10.3390/antiox9090901 [PubMed: 32971909]

Opie LH (2014). Cardiac Metabolism in Health and Disease. In Cellular and Molecular Pathobiology of Cardiovascular Disease (pp. 23–36). Elsevier. 10.1016/B978-0-12-405206-2.00002-8

Palomo GM, & Manfredi G (2015). Exploring new pathways of neurodegeneration in ALS: The role of mitochondria quality control. Brain Research, 1607, 36–46. 10.1016/j.brainres.2014.09.065 [PubMed: 25301687]

Panchal K & Tiwari AK (2021). Miro (Mitochondrial Rho GTPase), a key player in mitochondrial axonal transport and mitochondrial dynamics in neurodegenerative diseases. Mitochondrion, 56, 118–135. 10.1016/i.mito.2020.10.005 [PubMed: 33127590]

Author Manuscript

Author Manuscript

Author Manuscript

Author Manuscript

Pandey UB, & Nichols CD (2011). Human Disease Models in *Drosophila melanogaster* and the Role of the Fly in Therapeutic Drug Discovery. Pharmacological Reviews, 63(2), 411–436. 10.1124/pr.110.003293 [PubMed: 21415126]

Phillips JP, Tainer JA, Getzoff ED, Boulianne GL, Kirby K, & Hilliker AJ (1995). Subunit-destabilizing mutations in Drosophila copper/zinc superoxide dismutase: Neuropathology and a model of dimer dysequilibrium. Proceedings of the National Academy of Sciences, 92(19), 8574–8578. 10.1073/pnas.92.19.8574

Phukan J, Pender NP, & Hardiman O (2007). Cognitive impairment in amyotrophic lateral sclerosis. The Lancet Neurology, 6(11), 994–1003. 10.1016/S1474-4422(07)70265-X [PubMed: 17945153]

Pickles S, Vigié P, & Youle RJ (2018). Mitophagy and Quality Control Mechanisms in Mitochondrial Maintenance. Current Biology, 28(4), R170–R185. 10.1016/j.cub.2018.01.004 [PubMed: 29462587]

Prudencio M, Hart PJ, Borchelt DR, & Andersen PM (2009). Variation in aggregation propensities among ALS-associated variants of SOD1: Correlation to human disease. Human Molecular Genetics, 18(17), 3217–3226. 10.1093/hmg/ddp260 [PubMed: 19483195]

Pugdahl K, Fuglsang-Frederiksen A, de Carvalho M, Johnsen B, Fawcett PRW, Labarre-Vila A, Liguori R, Nix WA, & Schofield IS (2006). Generalised sensory system abnormalities in amyotrophic lateral sclerosis: A European multicentre study. Journal of Neurology, Neurosurgery & Psychiatry, 78(7), 746–749. 10.1136/jnnp.2006.098533

Reis GF, Yang G, Szpankowski L, Weaver C, Shah SB, Robinson JT, Hays TS, Danuser G, & Goldstein LSB (2012). Molecular motor function in axonal transport in vivo probed by genetic and computational analysis in *Drosophila*. Molecular Biology of the Cell, 23(9), 1700–1714. 10.1091/mbc.e11-11-0938 [PubMed: 22398725]

Rikhy R, Kamat S, Ramagiri S, Sriram V, & Krishnan KS (2007). Mutations in dynamin-related protein result in gross changes in mitochondrial morphology and affect synaptic vesicle recycling at the Drosophila neuromuscular junction. Genes, Brain and Behavior, 6(1), 42–53. 10.1111/j.1601-183X.2006.00218.x [PubMed: 17233640]

Russo K, Spierer AN, & Wharton KA (2023) BMP signaling reduces motor dysfunction in knock-in Sod1 ALS model. Manuscript in preparation.

Sanyal S (2009). Genomic mapping and expression patterns of C380, OK6 and D42 enhancer trap lines in the larval nervous system of Drosophila. Gene Expression Patterns, 9(5), 371–380. 10.1016/j.gep.2009.01.002 [PubMed: 19602393]

Saccon RA, Bunton-Stasyshyn RKA, Fisher EMC, & Fratta P (2013). Is SOD1 loss of function involved in amyotrophic lateral sclerosis? Brain, 136(8), 2342–2358. 10.1093/brain/awt097 [PubMed: 23687121]

ahin A, Held A, Bredvik K, Major P, Achilli T-M, Kerson AG, Wharton K, Stilwell G, & Reenan R (2017). Human SOD1 ALS Mutations in a *Drosophila* Knock-In Model Cause Severe Phenotypes and Reveal Dosage-Sensitive Gain- and Loss-of-Function Components. Genetics, 205(2), 707–723. 10.1534/genetics.116.190850 [PubMed: 27974499]

Sasaki S (2011). Autophagy in Spinal Cord Motor Neurons in Sporadic Amyotrophic Lateral Sclerosis. Journal of Neuropathology & Experimental Neurology, 70(5), 349–359. 10.1097/NEN.0b013e3182160690 [PubMed: 21487309]

Sayers EW, Bolton EE, Brister JR, Canese K, Chan J, Comeau DC, Connor R, Funk K, Kelly C, Kim S, Madej T, Marchler-Bauer A, Lanczycki C, Lathrop S, Lu Z, Thibaud-Nissen F, Murphy T, Phan L, Skripchenko Y, … Sherry ST (2022). Database resources of the national center for biotechnology information. Nucleic Acids Research, 50(D1), D20–D26. 10.1093/nar/gkab1112 [PubMed: 34850941]

Schafer FQ, & Buettner GR (2001). Redox environment of the cell as viewed through the redox state of the glutathione disulfide/glutathione couple. Free Radical Biology and Medicine, 30(11), 1191–1212. 10.1016/S0891-5849(01)00480-4 [PubMed: 11368918]

Schapira AHV, & Cooper JM (1992). Mitochondrial function in neurodegeneration and ageing. Mutation Research/DNAging, 275(3–6), 133–143. 10.1016/0921-8734(92)90018-K

Shen Q, Yamano K, Head BP, Kawajiri S, Cheung JTM, Wang C, Cho J-H, Hattori N, Youle RJ, & van der Bliek AM (2014). Mutations in Fis1 disrupt orderly disposal of defective mitochondria. Molecular Biology of the Cell, 25(1), 145–159. 10.1091/mbc.e13-09-0525 [PubMed: 24196833]

Sheng Y, Chattopadhyay M, Whitelegge J, & Valentine JS (n.d.). SOD1 Aggregation and ALS: Role of Metallation States and Disulfide Status. Current Topics in Medicinal Chemistry, 12(22), 2560–2572. Retrieved January 19, 2023, from https://www.eurekaselect.com/article/49794

Shimada S, Oosaki M, Takahashi R, Uene S, Yanagisawa S, Tsukihara T, & Shinzawa-Itoh K (2018). A unique respiratory adaptation in Drosophila independent of supercomplex formation. Biochimica et Biophysica Acta (BBA) - Bioenergetics, 1859(2), 154–163. 10.1016/j.bbabio.2017.11.007 [PubMed: 29191512]

Shimono K, Fujimoto A, Tsuyama T, Yamamoto-Kochi M, Sato M, Hattori Y, Sugimura K, Usui T, Kimura K, & Uemura T (2009). Multidendritic sensory neurons in the adult Drosophila abdomen: Origins, dendritic morphology, and segment- and age-dependent programmed cell death. Neural Development, 4(1), 37. 10.1186/1749-8104-4-37 [PubMed: 19799768]

Smith EF, Shaw PJ, & De Vos KJ (2019). The role of mitochondria in amyotrophic lateral sclerosis. Neuroscience Letters, 710, 132933. 10.1016/j.neulet.2017.06.052 [PubMed: 28669745]

Solesio ME, Prime TA, Logan A, Murphy MP, del Mar Arroyo-Jimenez M, Jordán J, & Galindo MF (2013). The mitochondria-targeted anti-oxidant MitoQ reduces aspects of mitochondrial fission in the 6-OHDA cell model of Parkinson's disease. Biochimica et Biophysica Acta (BBA) - Molecular Basis of Disease, 1832(1), 174–182. 10.1016/j.bbadis.2012.07.009 [PubMed: 22846607]

Song W, Onishi M, Jan LY, & Jan YN (2007). Peripheral multidendritic sensory neurons are necessary for rhythmic locomotion behavior in Drosophila larvae. Proceedings of the National Academy of Sciences, 104(12), 5199–5204. 10.1073/pnas.0700895104

Spillane M, Ketschek A, Merianda TT, Twiss JL, & Gallo G (2013). Mitochondria Coordinate Sites of Axon Branching through Localized Intra-axonal Protein Synthesis. Cell Reports, 5(6), 1564–1575. 10.1016/j.celrep.2013.11.022 [PubMed: 24332852]

Sultan AA, Waller R, Heath PR, & Kirby J (2016, May 13). The genetics of amyotrophic lateral sclerosis: Current insights. Degenerative Neurological and Neuromuscular Disease. 10.2147/DNND.S84956

Tafuri F, Ronchi D, Magri F, Comi GP, & Corti S (2015). SOD1 misplacing and mitochondrial dysfunction in amyotrophic lateral sclerosis pathogenesis. Frontiers in Cellular Neuroscience, 9. 10.3389/fncel.2015.00336

Taylor JP, Brown RH, & Cleveland DW (2016). Decoding ALS: From genes to mechanism. Nature, 539(7628), 197–206. 10.1038/nature20413 [PubMed: 27830784]

Tissot M, & Stocker RF (2000). Metamorphosis in Drosophila and other insects: The fate of neurons throughout the stages. Progress in Neurobiology, 62(1), 89–111. 10.1016/S0301-0082(99)00069-6 [PubMed: 10821983]

Tsang CK, Liu Y, Thomas J, Zhang Y, & Zheng XFS (2014). Superoxide dismutase 1 acts as a nuclear transcription factor to regulate oxidative stress resistance. Nature Communications, 5(1), 3446. 10.1038/ncomms4446

Valentine JS, Doucette PA, & Zittin Potter S (2005). COPPER-ZINC SUPEROXIDE DISMUTASE AND AMYOTROPHIC LATERAL SCLEROSIS. Annual Review of Biochemistry, 74(1), 563–593. 10.1146/annurev.biochem.72.121801.161647

Vande Velde C, McDonald KK, Boukhedimi Y, McAlonis-Downes M, Lobsiger CS, Bel Hadj S, Zandona A, Julien J-P, Shah SB, & Cleveland DW (2011). Misfolded SOD1 Associated with Motor Neuron Mitochondria Alters Mitochondrial Shape and Distribution Prior to Clinical Onset. PLoS ONE, 6(7), e22031. 10.1371/journal.pone.0022031 [PubMed: 21779368]

Vaughan SK, Kemp Z, Hatzipetros T, Vieira F, & Valdez G (2015). Degeneration of proprioceptive sensory nerve endings in mice harboring amyotrophic lateral sclerosis-causing mutations: Proprioceptive Sensory Neurons and ALS. Journal of Comparative Neurology, 523(17), 2477–2494. 10.1002/cne.23848 [PubMed: 26136049]

Vos M (2010). Synaptic mitochondria in synaptic transmission and organization of vesicle pools in health and disease. Frontiers in Synaptic Neuroscience, 2. 10.3389/fnsyn.2010.00139

Weinrich TW, Kam JH, Ferrara BT, Thompson EP, Mitrofanis J, & Jeffery G (2019). A day in the life of mitochondria reveals shifting workloads. Scientific Reports, 9(1), 13898. 10.1038/s41598-019-48383-y [PubMed: 31554906]

Wijesekera LC, & Nigel Leigh P (2009). Amyotrophic lateral sclerosis. Orphanet Journal of Rare Diseases, 4(1), 3. 10.1186/1750-1172-4-3 [PubMed: 19192301]

Williams DW, & Truman JW (2005). Cellular mechanisms of dendrite pruning in *Drosophila*: Insights from in vivo time-lapse of remodeling dendritic arborizing sensory neurons. Development, 132(16), 3631–3642. 10.1242/dev.01928 [PubMed: 16033801]

Woolsey PBE (2008). Cysteine, Sulfite, and Glutamate Toxicity: A Cause of ALS? The Journal of Alternative and Complementary Medicine, 14(9), 1159–1164. 10.1089/acm.2007.0781 [PubMed: 18973429]

Xu J, Du W, Zhao Y, Lim K, Lu L, Zhang C, & Li L (2022). Mitochondria targeting drugs for neurodegenerative diseases—Design, mechanism and application. Acta Pharmaceutica Sinica B, 12(6), 2778–2789. 10.1016/j.apsb.2022.03.001 [PubMed: 35755284]

Youle RJ, & van der Bliek AM (2012). Mitochondrial Fission, Fusion, and Stress. Science, 337(6098), 1062–1065. 10.1126/science.1219855 [PubMed: 22936770]

Zanette G, Tamburin S, Manganotti P, Refatti N, Forgione A, & Rizzuto N (2002). Changes in motor cortex inhibition over time in patients with amyotrophic lateral sclerosis. Journal of Neurology, 249(12), 1723–1728. 10.1007/s00415-002-0926-7 [PubMed: 12529797]

Žďarek J, & Friedman S (1986). Pupal ecdysis in flies: Mechanisms of evagination of the head and expansion of the thoracic appendages. Journal of Insect Physiology, 32(11), 917–923. 10.1016/0022-1910(86)90139-3

Zhu C, Beck V, Griffith JD, Deshmukh M, Dokholyan NV (2018) Large SOD1 aggregates, unlike trimeric SOD1, do not impact cell viability in a model of amyotrophic lateral sclerosis. Proc. Natl. Acad. Sci, 115 (18), 4661–4665. 10.1073/pnas.1800187115 [PubMed: 29666246]
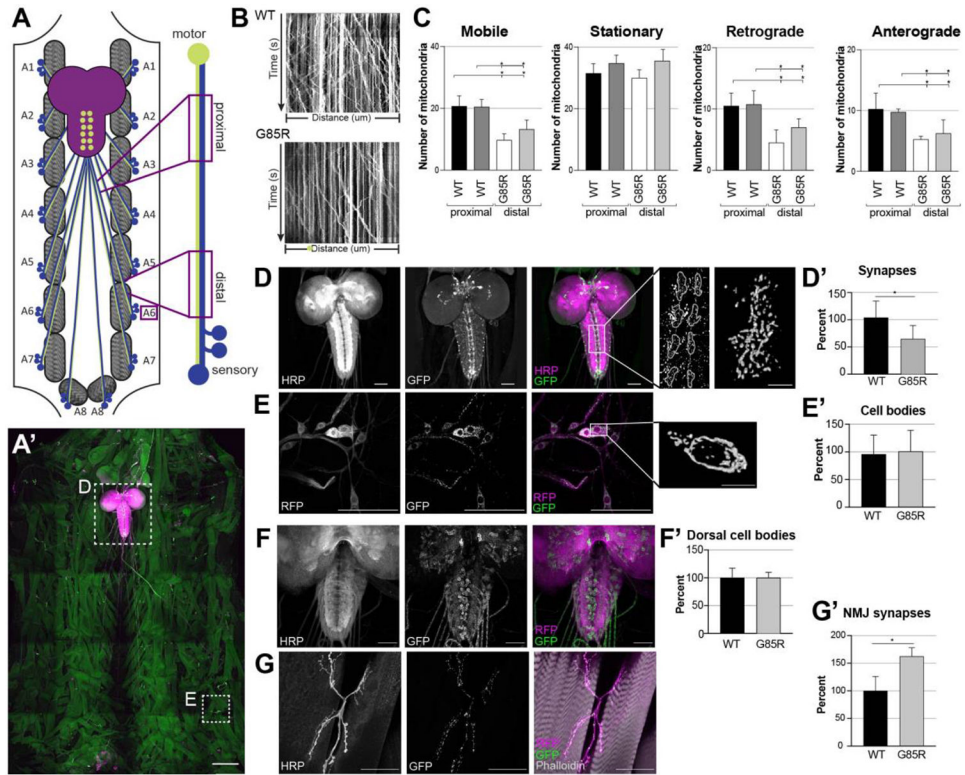
Figure 1:

Abnormal mitochondrial content in compartments of sensory and motor neurons in *dSod1*^{G85R}.

(A) Schematic of 3rd instar larval filet, CNS (brain and VNC, purple), a segmentally arranged muscle (gray hatching), and segmental nerves composed of motor (green) projecting to muscles, and sensory (blue) axons projecting from the peripherally located cell bodies to the VNC; boxed areas show proximal and distal regions of the A6 segmental nerve that were imaged, **(A')** tiled confocal micrograph shows organization of body wall musculature (faint green), CNS (brain lobes and ventral nerve cord (VNC) stained with HRP (magenta; dashed box, high mag shown in **D**) and MD>mito-GFP (bright green) of a *dSod1*^{G85R} larval filet. **(B)** Kymographs depicting live imaging of mito-GFP over time within a proximal region of the MD sensory axon in *dSod1*^{WT} (top, control) and *dSod1*^{G85R} (bottom). Vertical lines indicate fluorescent signal for stationary mitochondria, diagonal lines are indicative of mitochondria that moved in retrograde or anterograde direction within the imaging window (distance). **(C)** Quantification of mito-GFP puncta from live imaging in the proximal and distal regions of MD axons (MD>mito-GFP) in segmental nerve A6 in *dSod1*^{WT} and *dSod1*^{G85R} 3rd instar larvae (WT and G85R n=4). Ordinary one-way ANOVA with Tukey's multiple comparison test. (*) = p-value <0.05. **(D)** Neurons labelled with anti-horseradish peroxidase (HRP) (gray, magenta) and mitochondria in MD synaptic regions, ladder-like midline of VNC (gray, green) in *MD-Gal4 UAS-mito-GFP*. Higher magnification of synaptic regions in midline with mitochondrial volume image of a single synaptic region (scale bar = 5um). **(E)** cell bodies of MD class IV da neurons marked by MD>*mcd8-RFP* (RFP) and mitochondria (mito-GFP); Higher magnification shows a

mitochondrial volume image of single cell body (scale bar = 10um). **(D',E')** Quantification of mitochondria at MD synapses and cell bodies in *dSod1*[G85R] as percent of WT; WT n=39 larvae, G85R n=52 larvae. **(F)** *dSod1*[G85R] VNC showing neuropil (anti-HRP, magenta) and mitochondria in motor neurons (*OK6-Gal4 mito-GFP,* green). **(G)** body wall muscles 6 and 7 in hemisegment A2 (phalloidin, magenta) with synaptic neuromuscular junction (NMJ) structure (NMJ 6/7) and mitochondria (green) labelled; all images are 40X objective magnification, not tiled. **(F',G')** Quantifications of mito-GFP puncta show changes in cell bodies and NMJs of OK6 motor neurons; WT and G85R n=4; each datapoint represents quantifications from one larva, as percent of WT. Scale bars = 50um unless labelled otherwise. Statistical analysis with student's t-test, (*) p-value <0.05. Full genotypes in Table 1.
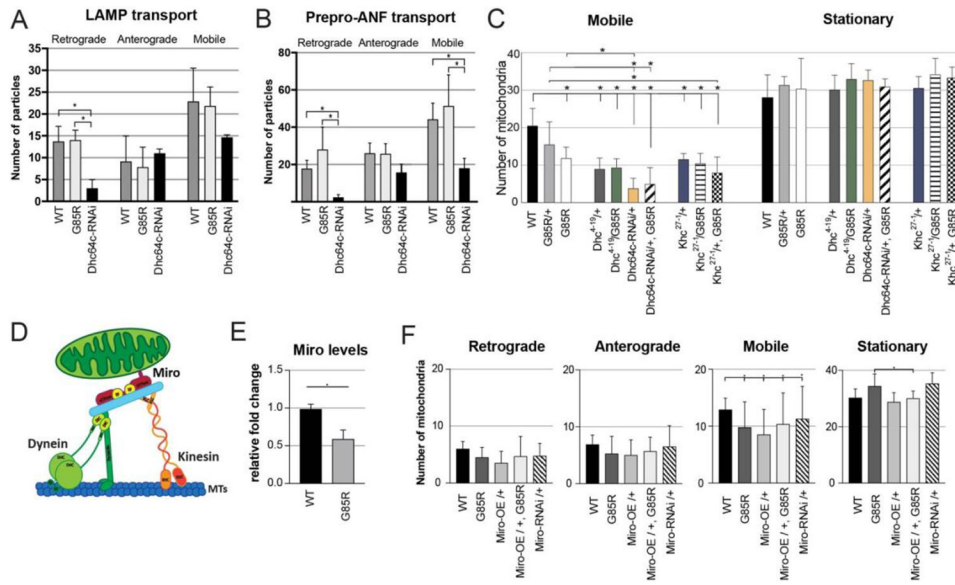
Figure 2:
General disruption of axonal transport machinery not affected in *dSod1G85R*. Quantification of live imaging of **(A)** lysosomal associated membrane protein 1 (LAMP-GFP) and **(B)** vesicles containing atrial natriuretic factor (preproANF-Emerald) in MD axon A6 in *dSod1WT* (WT), *dSod1G85R* (G85R), and MD-expressed dynein heavy chain RNAi (*Dhc64c-RNAi*). LAMP-GFP,WT and LAMP-GFP,G85R (n=8); preproANF-Emerald,WT and prepro-ANF-Emerald,G85R (n=4). (**C**) Number of mobile versus stationary mitochondria (mito-GFP) observed by live imaging of MD axons quantified following genotypes: WT (n=19), G85R/+ (n=7), G85R (n=20), Dhc4-19 /+ (n=6), Dhc4-19 /G85R (n=5), Dhc64c-RNAi/+ (n=7), Dhc64c-RNAi/+, G85R (n=3), Khc27-1 /+ (n=6), Khc4/19 / G85R (n=4), Khc4/19 /+, G85R (n=5); (**D**) Schematic of mitochondrial transport machinery show microtubule (MTs) motor proteins dynein and kinesin and the adaptor Miro. Adapted from Schwarz 2019. (**E**) *Miro* expression level based on qPCR in G85R compared to WT whole larvae; n=6 larvae; Students' t-test. (**F**) Quantification of live-imaging mito-GFP, when the *Miro* adaptor protein is overexpressed (Miro-OE) or downregulated (Miro-RNAi) in *dSod1WT* (WT) or *dSod1G85R* (G85R). WT (n =8), G85R (n=8), Miro-OE/+ (n=4), Miro-OE/+, G85R (n=4), Miro-RNAi /+ (n=4). Ordinary one-way ANOVA with Tukey's multiple comparison test, (*) p-value <0.05. Full genotypes in Table 1.
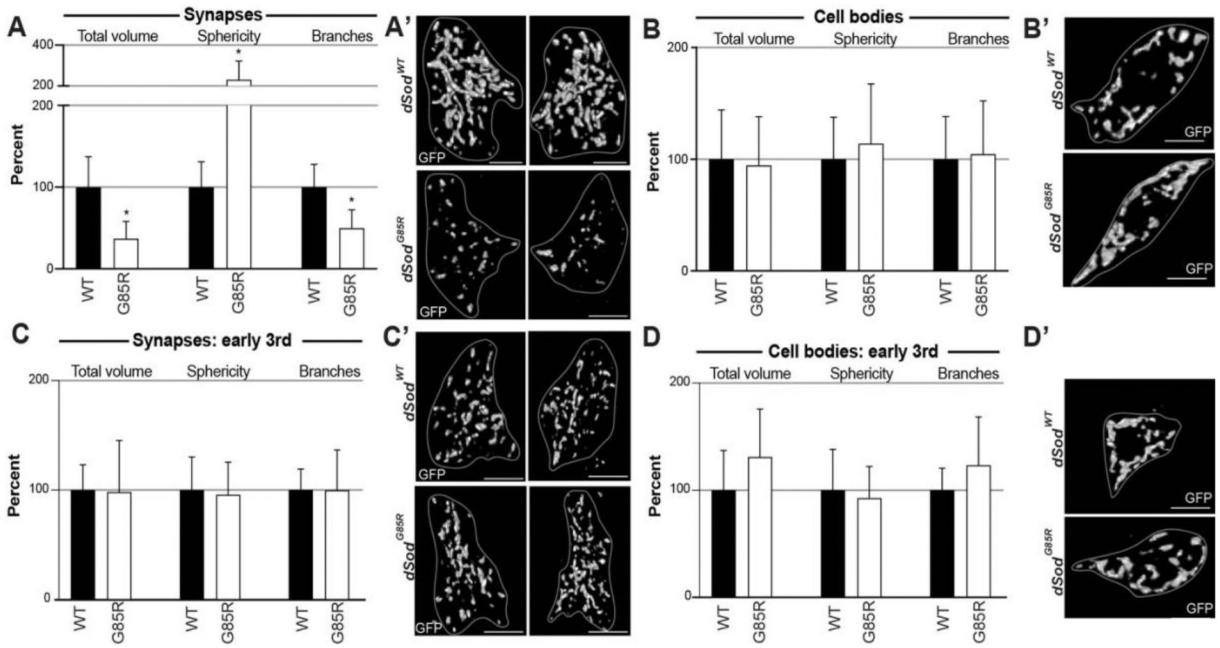
Figure 3:

Altered mitochondrial morphology in *dSod1^{G85R}* MD neurons. Synaptic termini in the VNC corresponding to A6 **(A,C)** and cell bodies **(B,D)** of mitochondria in MD neurons of wandering **(A,B)** and early **(C,D)** 3rd instar larvae. A subset of quantified parameters is shown in each case for *dSod1^{WT}* (WT, black bars) and *dSod1^{G85R}* (G85R, white bars), with **(A)** WT n=18, G85R n=10, **(B)** WT n=18, G85R n=14, **(C)** WT n=7, G85R n=6, **(D)** WT n=7, G85R n=6. Full genotypes denoted in Table 1. Scale bar = 5um for synapses, 10um for cell bodies. Student's t-test with a (*) p-value <0.05. Full dataset from Mitochondria-Analyzer analysis in Supp 6.
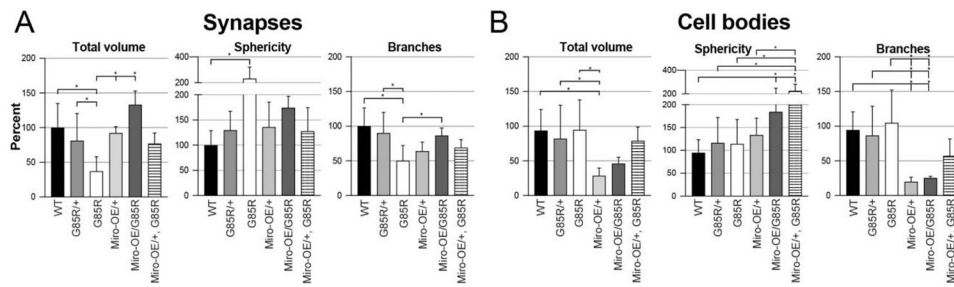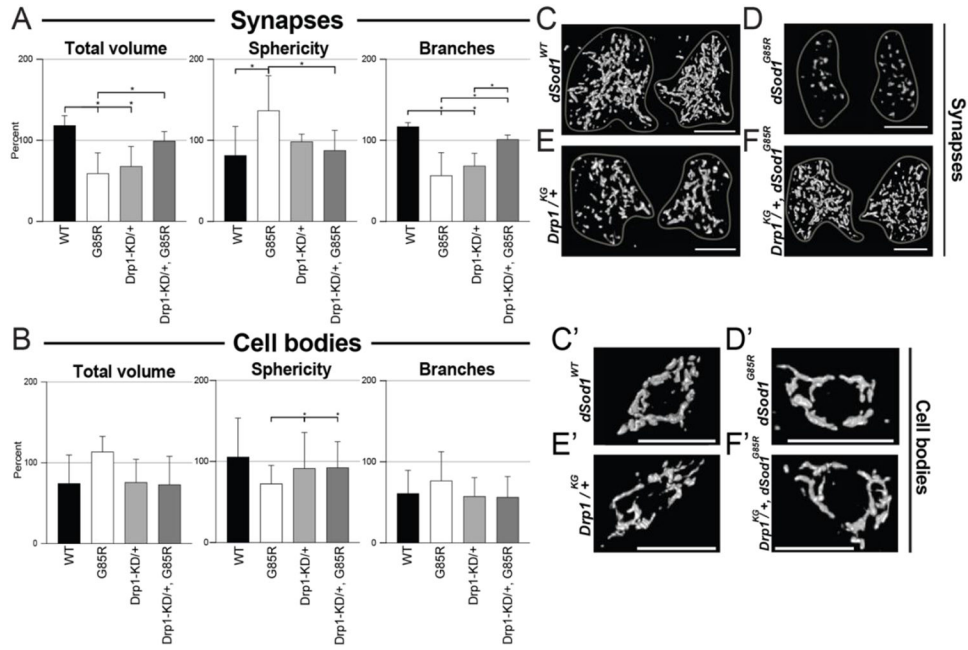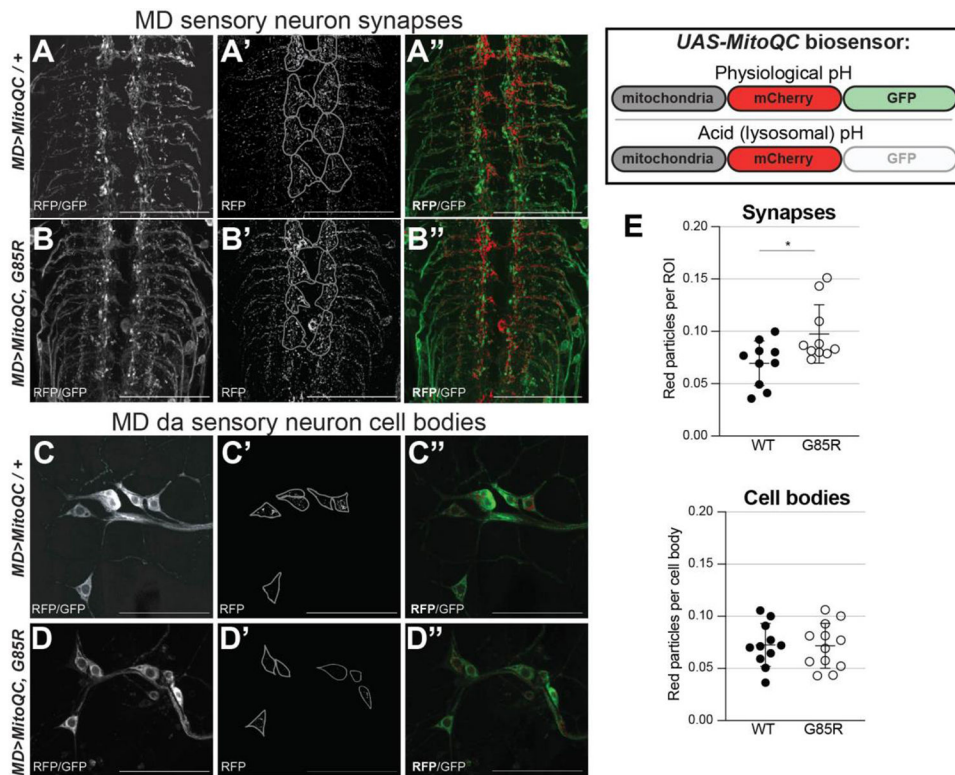
Figure 4:

Genetic interaction between *Miro* and *dSod1*^{G85R} observed in MD neurons when assessing mitochondrial morphology. Quantifications in synapses **(A)** and cell bodies **(B)** of MD neurons in *dSod1*^{G85R} larvae showing total volume, sphericity, and branches. **(A)** synapses: WT (n=21), G85R/+ (n=15), G85R (n=8), Miro-OE/+ (n=7), Miro-OE/G85R (n=4), Miro-OE/+, G85R (n=6) **(B)** cell bodies: WT (n=20), G85R/+ (n=18), G85R (n=15), Miro-OE/+ (n=7), Miro-OE/G85R (n=5), Miro-OE/+, G85R (n=6). Statistical analyses done with ordinary one-way ANOVA with Tukey's multiple comparison test; (*) p-value <0.05. All data from Mitochondrial Analyzer in Supp 5. Full genotypes in Table 1.

Figure 5:

Drp1 knockdown rescues mitochondrial morphology defects in *dSod1^G85R^* MD synapses. **(A,B)** Quantification of mitochondrial total volume, sphericity, and branches in MD neurons of *dSod1^G85R^* larvae in relation to the functional null fission factor Drp1, *Drp1^KG03815^*, in synapses **(A)** of WT (n=4), G85R (n=9), Drp1-KD/+ (n=5), and Drp1-KD/+, G85R (n=6) 3rd instar larva, and cell bodies **(B)** of WT (n=8), G85R (n=8), Drp1-KD/+ (n=6), and Drp1-KD/+, G85R (n=6) 3rd instar larva. **(C-F)** 3D reconstruction of synaptic mitochondria at segments A2 of the VNC, left and right side, **(C'-F')** 3D reconstruction of mitochondrial at cell bodies of ddaE cell in the *da* cluster. Ordinary one-way ANOVA with Tukey's multiple comparison test; (*) p-value <0.05. All data from Mitochondrial Analyzer plugin in Supp 9.

Figure 6:

Increased mitophagy at synapses of MD neurons in *dSod1*^{G85R}. *MitoQC*, a biosensor for mitophagy, fluoresces in both red and green channels under physiological (top) conditions, but only in red under acidic conditions (bottom), such as in mitolysosomes. Immunocytochemistry of axon terminals **(A-B")** of A3-A6 VNC segments and cell bodies **(C-D")** in segment A3 of MD neurons expressing *mitoQC* biosensor. From left to right images are showing GFP and RFP composite, thresholded and RFP isolated, thresholded RFP and GFP alone. **(E)** Graphs show particles of RFP (mitolysosomes) normalized to synaptic (top) and to cell body (bottom) areas. Statistical analysis with Students' t-test; scale bars at 50um; images are taken with a 63Xoil objective; (*) p-value <0.05.
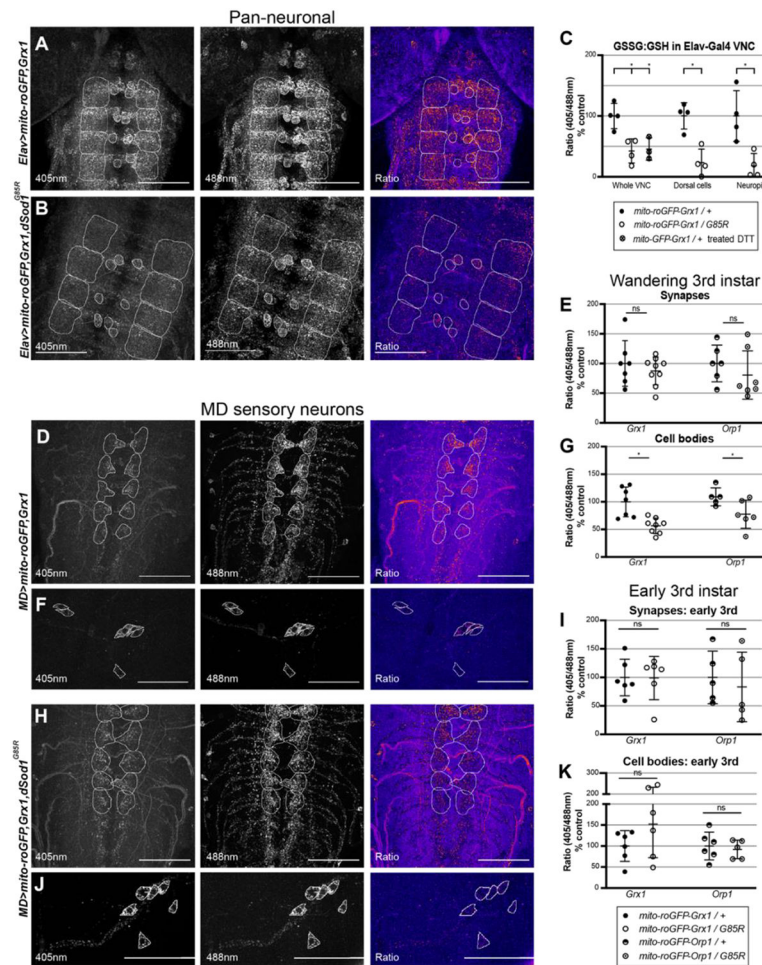
Figure 7:

Levels of glutathione redox couple and hydrogen peroxide are altered in cell bodies of MD neurons in *dSod1^(G85R)*. Innate fluorescence images of **(A,D,H)** axon terminals of A2-A6 VNC segments and **(F,J)** cell bodies in segment A2 of neurons expressing *mito-roGFP,Grx1* biosensor in the WT background; **(B)** and **(H,J)** show the biosensor in *dSod1^(G85R)*. From left to right, panels are 405nm, 488nm, and the ratio panel highlights differences between 405nm and 488nm. **(A-B)** VNCs of pan-neuronal ELAV driver expressing *mito-roGFP,Grx1*. White outlines highlight dorsal cells and neuropil in VNC segments A3-A6. **(C)** Graph showing levels of GSSG:GSH (Grx1 probe) in whole VNC, dorsal cells, and neuropil. VNCs treated with DTT reductant serve as a control for effectiveness of probe. Levels of GSSG:GSH (Grx1 probe) and H_2O_2 (Orp1 probe) redox couples in synapses **(D,H,E)** and cell bodies **(F,J,G)** of MD neurons of wandering 3^(rd) instar, and in synapses **(I)** and cell bodies **(J)** of MD neurons in early 3^(rd) instar larvae. Students' t-test, (*) p-value <0.05.
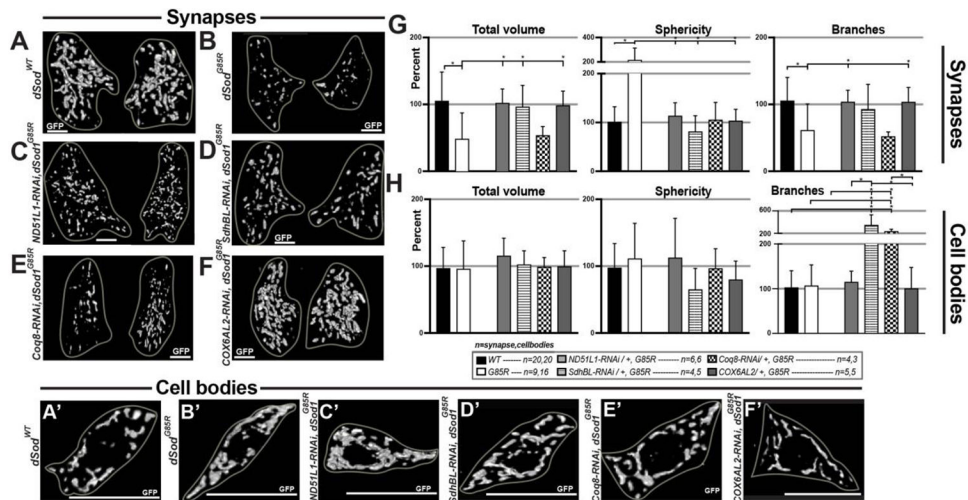
Figure 8:

Knocking down complex I, II, and IV subunits ameliorates mitochondrial morphological defects in *dSod1*^{G85R} MD neurons. **(A-F)** 3D reconstructions of synaptic mitochondria at segment A2 of the VNC – left and right side. All graphs show total volume, sphericity, and branches of mitochondria in synapses and in cell bodies. Mitochondria in synapses **(G)** and cell bodies **(H)** in WT, G85R, ND51L1-RNAi/+, G85R; SdhBL-RNAi/+, G85R; Coq8-RNAi/+, G85R; COX6AL2-RNAi/+, G85R. Sample n shown in figure as n in "synapses, cell bodies." Statistical analysis: one-way ANOVA with Tukey's multiple comparison test on normally distributed data, Kruskal-Wallis test with a Dunn correction for multiple comparisons on non-normally distributed data; (*) p-value <0.05. Scale bars are 10um. All data from Mitochondrial Analyzer plugin in Supp 9. Full genotypes in Methods section.
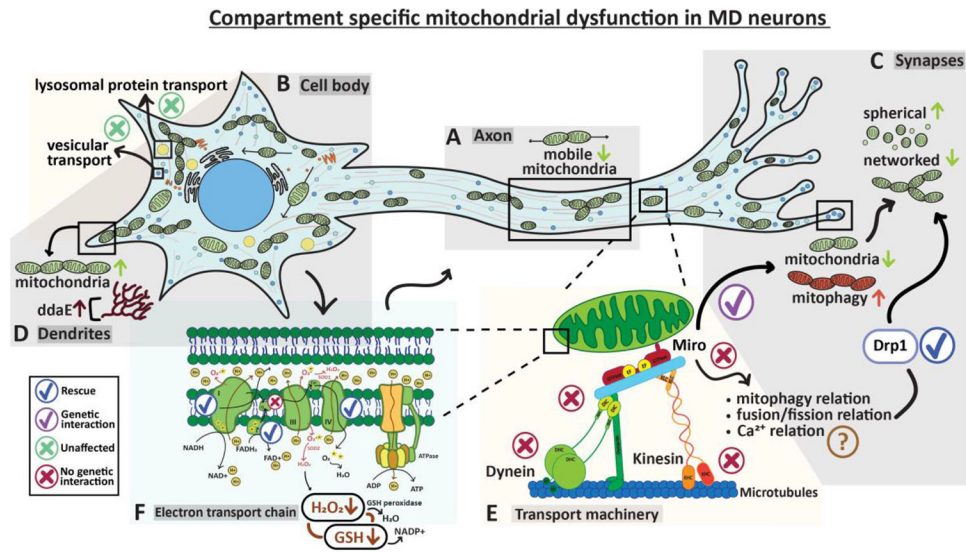
Figure 9: Mitochondrial number, morphology, and function exhibit compartment-specific abnormalities in MD sensory neurons of the *dSod1*^{G85R}-knock-in ALS model.
Schematic summarizes results presented. **(A)** A decrease in mobile mitochondria is evident in axons (Fig 1) with no change in transport of lysosomes or dense core vesicles (Fig 2). **(B)** No morphological changes in mitochondria observed in cell bodies. Distribution and overall number of lysosomes and dense core vesicles are unchanged across the neuronal compartments – Fig 1,3. **(C)** Decrease in overall mitochondria content at synaptic regions accompanied by an increase in mitochondrial turnover (mitophagy). In addition, synaptic mitochondria are more spherical and less networked. Knock down of fission factor *Drp1* can rescue morphological defects -- Figures 1,3,4. **(D)** Mitochondrial content in MD dendrites is altered and accompanied by structural changes in ddaE – Supp 1. **(E)** Mitochondrial transport was unaffected (X) in genetic combination of *dSod1*^{G85R} heterozygote and mutations in *dynein, kinesin*, and *Miro* suggesting that axonal transport machinery is not inherently defective in the ALS model (Fig 2). Schematic adapted from Schwarz, 2019. While mitochondrial movement is unaffected when manipulating *Miro* in a *dSod1*^{G85R} background, mitochondrial morphology is rescued, suggesting that fission and fusion dynamics, mitophagy, and calcium buffering are more likely disrupted in *dSod1*^{G85R}-ALS than the axonal transport machinery (Figures 1,2,3,4). **(F)** Levels of redox couple GSSG:GSH and H_2O_2 reduced in cell bodies indicating compromised mitochondrial function. Knockdown of ETC subunit ND51L (Complex I), SdhBL (Complex II), or COX6AL2 (Complex IV), rescues morphological defects found at synapses and changes mitochondrial structure at cell bodies(Fig 7,8). Manipulating coenzyme Q did not rescue (X). Overall, *dSod1*^{G85R}-ALS sensory neurons exhibit compartment-specific mitochondrial defects which can be ameliorated by manipulating ETC subunits and *Drp1* fission factor.

Table 1:

Full genotypes by figure

Figure 1	Comments
w; MD-Gal4/+; UAS-mitoGFP +/+ dSod1^{WT}	*MD-Gal4* - BSC #8769; *UAS-mitoGFP* - BSC #8443; *dSod1$^{WT-loxP}$*
w; MD-Gal4/+; UAS-mitoGFP dSod1^{G85R}/+ dSod1^{G85R}	Homozygous *dSod1$^{G85R-hr}$*
w; OK6-Gal4/+; UAS-mitoGFP +/+ dSod1^{WT}	*OK6-Gal4*, generous donation from Heather Broihier; *dSod1$^{WT-loxP}$*
w; OK6-Gal4/+; UAS-mitoGFP dSod1^{G85R}/+ dSod1^{G85R}	Homozygous *dSod1$^{G85R-hr}$*
Supp 1	**Comments**
w; MD-Gal4 UAS-mcd8. RFP/+; +/ dSod1^{WT}	*MD-Gal4* - BSC #8769; *UAS-mcd8RFP* - BSC #27398; *dSod1$^{WT-loxP}$*
w; MD-Gal4 UAS-mcd8. RFP/+; dSod1^{G85R}/dSod1^{G85R}	Homozygous *dSod1$^{G85R-hr}$*
Figure 2, Supp 2, 3	**Comments**
w; MD-Gal4/+; UAS-LAMP-GFP +/+ dSod1^{WT}	*UAS-LAMP-GFP*, generous donation from Helmut Kramer; *dSod1$^{WT-loxP}$*
w; MD-Gal4/+; UAS-LAMP-GFP dSod1^{G85R} /+ dSod1^{G85R}	Homozygous *dSod1$^{G85R-hr}$*
w; MD-Gal4/+; UAS-LAMP-GFP/UAS-Dhc64c-RNAi	*UAS-Dhc64c-RNAi* - BSC#36698
w; MD-Gal4/ UAS-preproANF-Emerald; +	*UAS-preproANF-Emerald* – BSC#7001; *dSod1^{WT-cr}*
w; MD-Gal4/ UAS-preproANF-Emerald; dSod1^{G85R}/dSod1^{G85R}	Homozygous *dSod1$^{G85R-cr}$*
w; MD-Gal4/+; UAS-preproANF-Emerald/UAS-Dhc64c-RNAi	
w; MD-Gal4/+; UAS-mitoGFP +/+ dSod1^{WT}	*dSod1^{WT-cr}* (Supp 2)
w; MD-Gal4/+; UAS-mitoGFP +/+ dSod1^{G85R}	*dSod1$^{G85R-hr}$*
w; MD-Gal4/+; UAS-mitoGFP dSod1^{G85R}/+ dSod1^{G85R}	Homozygous *dSod1$^{G85R-cr}$*
w; MD-Gal4/+; UAS-mitoGFP/UAS-Dhc$^{4-19}$	*UAS-Dhc$^{4-19}$* gift from Tom Hays
w; MD-Gal4/+; UAS-mitoGFP dSod1^{G85R}/+ UAS-Dhc$^{4-19}$	*dSod1$^{G85R-cr}$*
w; MD-Gal4/+; UAS-mitoGFP/UAS-Dhc64c-RNAi	*UAS-Dhc64c-RNAi* - BSC#36698
w; MD-Gal4/+; UAS-mitoGFP dSod1^{G85R}/UAS-Dhc64c-RNAi dSod1^{G85R}	Homozygous *dSod1$^{G85R-cr}$*
w; MD-Gal4/+; UAS-mitoGFP/UAS-Khc$^{27-1}$	*UAS-Khc$^{27-1}$* – BSC #67409
w; MD-Gal4/+; UAS-mitoGFP dSod1^{G85R}/+ UAS-Khc$^{27-1}$	*dSod1$^{G85R-hr}$*
w; MD-Gal4/+; UAS-mitoGFP/UAS-Khc$^{27-1}$ dSod1^{G85R}	Homozygous *dSod1$^{G85R-hr}$*
w; MD-Gal4/+; UAS-mitoGFP, dSod1^{WT} /UAS-Miro,	*UAS-Miro* – BSC #51646, *dSod1^{WT-cr}* (Supp 2, Supp 5)
w; MD-Gal4/+; UAS-mitoGFP, dSod1^{G85R} /UAS-Miro, dSod1^{G85R}	Homozygous *dSod1$^{G85R-cr}$* (Supp 5)
w; MD-Gal4/+; UAS-mitoGFP/UAS-Miro-RNAi	*UAS-Miro-RNAi* – BSC #27695
Supp 4	**Comments**
w; MD-Gal4/+; UAS-mitoGFP + /+ dSod1^{WT}	
w; MD-Gal4/+; + /UAS-mitoGFP dSod1^{G85R}	
w; MD-Gal4/+; + dSod1^{G85R}/UAS-mitoGFP dSod1^{G85R}	Homozygous *dSod1$^{G85R-hr}$*
w; MD-Gal4/+; + Dic^1/UAS-mitoGFP dSod^{WT}+	Dic^1 gift from Tom Hays
w; MD-Gal4/+; + Dic^1/UAS-mitoGFP dSod1^{G85R}+	

Figure 3, Supp 6	Comments
w; MD-Gal4/+; UAS-mitoGFP +/+ dSod1^{WT}	Wandering 3rd instar and early 3rd instar; *dSod1$^{WT-loxP}$* (Supp 3)
w; MD-Gal4/+; UAS-mitoGFP dSod1^{G85R}/+ dSod1^{G85R}	Wandering 3rd instar and early 3rd instar; homozygous *dSod1$^{G85R-hr}$* (Supp 3)
Figure 4, Supp 5, Supp 7	**Comments**
w; MD-Gal4/+; UAS-mitoGFP +/+ dSod1^{WT}	*dSod1^{WT-cr}*
w; MD-Gal4/+; UAS-mitoGFP +/+ dSod1^{G85R}	*dSod1$^{G85R-cr}$*
w; MD-Gal4/+; UAS-mitoGFP dSod1^{G85R}/+ dSod1^{G85R}	Homozygous *dSod1$^{G85R-cr}$*
w; MD-Gal4/+; UAS-mitoGFP dSod1^{WT}/+ UAS-Miro,	*UAS-Miro* – BSC #51646, *dSod1^{WT-cr}*
w; MD-Gal4/+; UAS-mitoGFP dSod1^{G85R} /UAS-Miro dSod1^{G85R}	Homozygous *dSod1$^{G85R-cr}$*
Figure 5, Supp 8	**Comments**
w; MD-Gal4/+; UAS-mitoGFP +/+ dSod1^{WT}	*dSod1$^{WT-loxP}$*
w; MD-Gal4/+; UAS-mitoGFP dSod1^{G85R}/+ dSod1^{G85R}	Homozygous *dSod1$^{G85R-hr}$*
w; MD-Gal4/ UAS-Drp1^{KG03815}; UAS-mitoGFP/+	*UAS-Drp1^{KG03815}* – BSC# 13510
w; MD-Gal4//UAS-Drp1^{KG03815}; UAS-mitoGFP dSod1^{G85R}/+ dSod1^{G85R}	Homozygous *dSod1$^{G85R-hr}$*
yw, Marf^{B}; MD-Gal4/+; UAS-mitoGFP/+	*Marf^{B}* – BSC# 67154
yw, Marf^{B}; MD-Gal4/+; UAS-mitoGFP + /+ dSod1^{G85R}	*dSod1$^{G85R-hr}$*
Figure 6	**Comments**
w; MD-Gal4, UAS-MitoQC/+; dSod1^{WT}/+	*UAS-MitoQC* was a generous donation from Alex Whitworth; *dSod1$^{WT-loxP}$*
w; MD-Gal4, UAS-MitoQC/+; dSod1^{G85R}/dSod1^{G85R}	Homozygous *dSod1$^{G85R-hr}$*
Figure 7	**Comments**
w; MD-Gal4/UAS-mito-roGFP-Grx1; dSod1^{WT}/+	For wandering 3rd instar and for early 3rd instar; *UAS-mito-roGFP2-Grx1* - BSC 67664; *dSod1^{WT-cr}*
w; MD-Gal4/UAS-mito-roGFP-Grx1; dSod1^{G85R}/dSod1^{G85R}	For wandering 3rd instar and for early 3rd instar; Homozygous *dSod1$^{G85R-cr}$*
w; MD-Gal4/UAS-mito-roGFP-Orp1; dSod1^{WT}/+	For wandering 3rd instar and for early 3rd instar; *UAS-mito-roGFP2-Orp1* - BSC 67673; *dSod1^{WT-cr}*
w; MD-Gal4/UAS-mito-roGFP-Orp1; dSod1^{G85R}/dSod1^{G85R}	For wandering 3rd instar and for early 3rd instar; Homozygous *dSod1$^{G85R-cr}$*
elav-Gal4; UAS-mito-roGFP,Grx1/+; dSod1^{WT}/+	*elav-Gal4 (C155-Gal4)* BSC #458; *dSod1^{WT-cr}*
elav-Gal4; UAS-mito-roGFP,Grx1/+; dSod1^{G85R}/dSod1^{G85R}	Homozygous *dSod1$^{G85R-hr}$*
Figure 8	**Comments**
w; MD-Gal4/+; UAS-mitoGFP +/+ dSod1^{WT}	*dSod1^{WT-cr}*
w; MD-Gal4/+; UAS-mitoGFP dSod1^{G85R}/+ dSod1^{G85R}	Homozygous *dSod1$^{G85R-cr}$*
w; MD-Gal4/UAS-ND51L1-RNAi; UAS-mitoGFP dSod1^{G85R}/+ dSod1^{G85R}	*UAS-ND51L1-RNAi* – BSC #42591
w; MD-Gal4/UAS-SdhBL-RNAi; UAS-mitoGFP dSod1^{G85R} /+ dSod1^{G85R}	*UAS-SdhBL-RNAi* – BSC 58100
w; MD-Gal4/UAS-Coq8-RNAi; UAS-mitoGFP dSod1^{G85R} /+ dSod1^{G85R}	*UAS-Coq8-RNAi* – BSC #57039
w; MD-Gal4/UAS-COX6AL2-RNAi; UAS-mitoGFP dSod1^{G85R} /+ dSod1^{G85R}	*UAS-COX6AL2-RNAi (CG14077-RNAi)* – BSC #53303

*
hr and loxP are the homologous recombination knock-in lines, cr is the CRISPR knock-in line

Table 2:

Genetic interactions between mutants in axons (transport assay) and in synapses (morphology assays) all in MD neurons. Table depicts whether a genetic interaction (GI) between a heterozygous mutant gene and heterozygous $dSod1^{G85R}/+$ is observed (yes – green), is trending towards significance (trend – yellow), or has no effect (red – NE). Genetic interactions were not determined for genotypes indicated with gray ND. Rescue in $dSod1^{G85R}$ columns depict whether expression of the heterozygous mutant in a homozygous $dSod1^{G85R}$ background rescues the defective phenotype observed. "Mobile mito" refers to mobile mitochondrial decrease in MD axons; "morpho" refers to changes in mitochondrial morphology, namely decreases in total volume and branches, and increases in sphericity.

| Genotype tested | | Genetic Interaction w/ G85R/+ | | | | Rescue of G85R/G85R | |
| | | *Transport* | *Mito morphology* | | | *Transport* | *Morphology* |
		mobile mito	total volume	sphericity	branching	mobile mito	vol, spheric branching
$Dhc^{A-19}/+$	Fig 2, Supp 3	NE	ND	ND	ND	ND	ND
$Dic^{J}/+$	Supp 4	NE	ND	ND	ND	ND	ND
$Khc^{27-1}/+$	Fig 2, Supp 3	NE	ND	ND	ND	NE	ND
$Miro\text{-}OE/+$	Figs 2, 4	NE	TREND	NE	TREND	NE	YES
$Drp1^{KG03815}/+$	Fig 5	ND	ND	ND	ND	ND	YES
$Marf^{B}/+$	Supp 8	ND	TREND	NE	NE	ND	NE
$ND51L1\text{-}RNAi/+$	Fig 8	ND	TREND	YES	NE	ND	YES
$SdhBL\text{-}RNAi/+$	Fig 8	ND	NE	NE	TREND	YES	YES
$Coq8\text{-}RNAi/+$	Fig 8	ND	ND	ND	ND	ND	SPHERICITY
$COX6AL2\text{-}RNAi/+$	Fig 8	ND	TREND	TREND	TREND	ND	YES